Meteorological Change and Impacts on Air Pollution – Results from North China

Ziping Xu[1], Song Xi Chen[2], Xiaoqing Wu[3]

[1]Yuanpei College, Peking University; Department of Statistics, University of Michigan, Ann Arbor, MI, USA
[2]Guanghua School of Management and
[2]Center for Statistical Science, Peking University, Beijing 100871, China
[3]Department of Geological & Atmospheric Sciences, Iowa State University, Ames, IA 50011, USA

Key Points:

- Meteorological changes led to 1.9 percent to 2.7 percent reduction in annual PM2.5 averages over North China 2014 to 2016 driven by temperature warming.
- Significant increases are detected in the surface temperature, boundary layer height and dissipation and decreases in relative humidity.
- The meteorological change should not be held responsible for the regional air pollution problem in North China.

Corresponding author: Song Xi Chen, csx@gsm.pku.edu.cn

This article has been accepted for publication and undergone full peer review but has not been through the copyediting, typesetting, pagination and proofreading process, which may lead to differences between this version and the Version of Record. Please cite this article as doi: 10.1029/2020JD032423

Abstract

There have been speculations that the severe air pollution experienced in North China was the act of meteorological change in general and a decreasing northerly wind in particular. We conduct a retrospective analysis on 1979-2016 reanalysis data from ERA-Interim of ECMWF over a region in North China to detect meteorological changes over the 38 years. No significant reduction in the northerly wind within the mixing layer is detected. Statistically significant increases are detected in the surface temperature, boundary layer height and dissipation, and significant decreases in relative humidity in the region between the first and second 19-year periods from 1979 to 2016. We build regression models of $PM_{2.5}$ on the meteorological variables using data in 2014, 2015 and 2016 to quantify effects of the meteorological changes between the two 19 years periods on $PM_{2.5}$ under the emission scenarios of 2014-2016. It is found that despite the warming, dew point temperature had been largely kept under control as the region had gotten dryer. This made the effects of temperature warming largely favorable to $PM_{2.5}$ reduction as it enhances boundary layer height and dissipation. It is found that the meteorological changes would lead to 1.29% to 2.76% reduction in annual $PM_{2.5}$ averages with January, March and December having more than 4% reduction in the three years. Thus, the meteorological change in North China had helped alleviate $PM_{2.5}$ to certain extent and should not be held responsible for the regional air pollution problem.

1 Introduction

A substantial part of China has experienced severe air pollution, and the region around the North China Plain (NCP) is the most severe. Air pollution is a major challenge faced by China as it tries to find a balance between economic growth and environmental sustainability. $PM_{2.5}$ [airborne particular matters (PM) with aerodynamic diameters less than $2.5\mu m$] has been the main air pollutant in China, whose main components are sulfate, nitrate, ammonium, organic carbon and elemental carbon. Epidemiological evidence shows that exposure to $PM_{2.5}$ can cause lung morbidity (Donaldson et al., 1998) and serious respiratory and cardiovascular diseases, and even death (Schwartz, 2000; Pope III et al., 2002; R. Chen et al., 2013).

The relationships between $PM_{2.5}$ and meteorological variables have been well studied in literature, such as in Tai et al. (2010, 2012) and Jacob and Winner (2009) in the context of climate change. Tai et al. (2012) revealed strong correlations between main species of $PM_{2.5}$ and temperature and relative humidity, respectively, using either the US EPA ground observations and simulated Geos-Chem grid data over the continental US. Jacob and Winner (2009) reviewed results from nine studies on the impacts of meteorological variables on $PM_{2.5}$. They used the perturbation analysis in Chemical Transportation Models (CTM) driven by General Circulation Model simulation (GCM) that mimicked various climate change scenarios. The review found that temperature, boundary layer height (BLH) and relative humidity had significant effects for $PM_{2.5}$, although the effects were weaker than those for the ozone, due to different components of the PM reacting differently to the meteorological conditions. Shen et al. (2018) and Pendergrass et al. (2019) revealed that winter $PM_{2.5}$ in Beijing was strongly correlated with the 850 hPa meridional wind velocity and the relative humidity. Stable synoptic and near-surface meteorological conditions were found to be strongly and positively associated with $PM_{2.5}$ concentration (Zheng et al., 2015; H. Chen & Wang, 2015; Miao et al., 2015). By analyzing data from the US Embassy, Liang et al. (2015) found that about 75% of $PM_{2.5}$'s variation in Beijing was driven by the meteorological factors. L. Chen et al. (2018) found the dew point temperature was more significant on $PM_{2.5}$ than the temperature and pressure based on air quality monitoring data in North China.

Climate change and its impacts on air pollution has been much investigated extensively in the literature. As summarized by Jacob and Winner (2009), existing studies can

be categorized as three approaches: (i) empirical correlation between PM and meteorological variables; (ii) perturbation analysis that perturb meteorological variables in regional Chemical Transport Models (CTM) so as to identify sensitive variables; and (iii) the General Circulation Model (GCM)-CTM simulation under various climate change scenarios. In particular, Tagaris et al. (2007) and Avise et al. (2009) projected declined $PM_{2.5}$ in year 2050 relative to that of year 2000 in the annual mean (-10%) and the July mean (-1 $\mu g/m^3$), respectively, in the US.

For the effects of climate change on China's air pollution, the results were mixed. There were studies projecting worsening air pollution under scenarios of climate change. H. Wang et al. (2015) found significant correlation between the number of winter haze days in eastern China with decreasing Arctic sea ice in the proceeding autumn based on 30 years' data from 1980s, and projected a worsening winter haze situation due to a northward shift of winter cyclone activity in East China (not focused on North China). Cai et al. (2017) found the winter haze days in Beijing were associated with northerly wind at 850 hPa, a dipole circulation pattern at 500 hPa, and temperature difference between the stratosphere and lower troposphere. By applying a statistical model to the future climate projections in the high emission scenario (Taylor et al., 2012), they found the circulation change induced by greenhouse gas emissions would contribute to more frequent haze days in Beijing from 2050 to 2100. In contrast, there were studies which predicted that the climate change was unlikely to significantly increase Beijing's $PM_{2.5}$ (Yin & Wang, 2016, 2017; Shen et al., 2018; Leung et al., 2018; Pendergrass et al., 2019). The number of winter haze days derived from the visibility observations in northern China displayed a decreasing trend from 1980 to 2012 and then this trend reverses after 2012 (Yin & Wang, 2016, 2017). Conclusions of both Shen et al. (2018) and Pendergrass et al. (2019) were based on the first principal component (PC) of the meteorological variables, which was dominated by the 850 hPa meridional wind velocity and the relative humidity, and had a strong explanation power on Beijing's $PM_{2.5}$. Shen et al. (2018) found that Beijing's $PM_{2.5}$ was directly dependent on a dipole structure in Arctic sea ice rather than the amount of sea ice, and the climate change effect was unable to reverse the effect of the current emission control effort in reducing Beijing's $PM_{2.5}$. And Pendergrass et al. (2019) indicated that climate change was unlikely to increase the frequency of severe $PM_{2.5}$ pollution events. Also based on the PC analysis, Leung et al. (2018) found that $PM_{2.5}$ in Beijing-Tianjin-Hebei region was highly dependent on the frequency of springtime Siberian highs and the relative humidity, and they projected a 0.46 $\pm$ 0.28 $\mu g/m^3$ reduction in 2050's annual $PM_{2.5}$ level relative to that of 2000's.

Our study contributes to the study on the effects of the climate changes on China's air pollution from a different perspective. It was motivated to empirically verify a speculation that the severe air pollution in North China was partly due to a weakening northerly wind as results of the meteorological change and wind energy development (Yan, 2015; Cheng, 2016). Two papers published in 2018 added more relevance to our study. X. Wang et al. (2018) found high aerosol loading as well as aerosols containing different elements encouraged tree growth. In another study, by simulations from the WRF-Chem model with emission inventory of 2013 and a module for the impacts of the surface roughness on the wind speed, Long et al. (2018) showed that the afforestation in the mountainous regions north and west of Beijing had contributed to a 6% increase in $PM_{2.5}$ in Beijing-Tianjin-Hebei region over the two-month period from December 2013 to January 2014.

Unlike most of the aforementioned studies on the climate changes, which are based on simulated projections via relevant models under certain emission and climate change and climate scenarios, this study takes a retrospect approach by obtaining realized meteorological changes and $PM_{2.5}$-meteorological relationship (rather than scenarios) embedded in the observations. Our study consists of three steps. In the first step, the realized pattern of the meteorological change are acquired by conducting statistical testing for changes in the ECMWF's reanalysis data between the two 19-year periods from

1979 to 2016 over 261 spatial grids of size 0.5×0.5 degree over a region in North China that encounters the most severe air pollution in the nation. In the second step, the emission scenarios of 2014 to 2016 are estimated by regression models between $PM_{2.5}$ and the meteorological variables based on data of the three years. Finally, we evaluate the impacts of the meteorological changes that happened from 1979 to 2016 on $PM_{2.5}$ concentration from 2014 to 2016 by substituting the meteorological means of the two 19 year periods to the fitted regression models of 2014-2016, respectively.

Our study cannot confirm diminishing northerly wind in the region from 1979 to 2016 as speculated, but finds instead significant temperature warming, drying, and increased boundary layer height and dissipation over the 38 year period from 1979 to 2016 in North China, which led to better vertical ventilation and a reducing effect on $PM_{2.5}$ as confirmed from the three year (2014-2016)'s regression models on the $PM_{2.5}$. Our calculation shows that the meteorological changes had actually decreased $PM_{2.5}$ in the majority of the months for most cities of the study region. Our results are in tune with the results of Shen et al. (2018); Leung et al. (2018); Pendergrass et al. (2019) confirming the "climate benefit", although we are focused on the past effects on 2014-2016's $PM_{2.5}$ while those three studies were focused on the projected effects in the future.

2 Data and Models

2.1 Study Region

The study region shown in Figure 1 ranges from 32.75° N to 42.75° N latitude and from 112.75° E to 119.75° E longitude excluding area over the sea. Located at the heart of North Central China that encompasses NCP and its surrounding areas, it covers a land area of 310,000 km^2 with a population exceeding 320 million which accounts for about 1/4 of China's population. In the last two decades, the region witnessed rapid industrialization and urbanization as well as chronic air pollution (Xu et al., 2013; Liang et al., 2015; Zhang et al., 2017).

2.2 Meteorological Data

We utilized a six-hourly gridded dataset, ERA-Interim of Global Reanalysis from ECMWF (Dee et al., 2011), which is produced with a data assimilation scheme advancing forward in time using 12-hourly analysis cycles. Starting from year 1979, the dataset has a spatial resolution of 0.5° latitude by 0.5° longitude, which results in 261 equal-size grids over the study region, excluding areas over the sea. The temporal frequency of the data is four times per day at 0200, 0800, 1400 and 2000 local time (LT). We choose ERA-Interim dataset because it contains the years 2014 to 2016 that cover the range of the available air quality data. We considered a time span up to the year 2016, which gives rise to 38 years of data. We evenly divide it into two periods: years 1979-1997 as Period 1 and years 1998-2016 as Period 2. Period 1 serves as the "control" period and Period 2 as the "treatment" period for the meteorological change. Incidentally, the year 1979 marked the first year of the economic reform in China, and the first period between 1979 to 1997 corresponded to a relatively slow pace of economic growth and industrialization, while the second period witnessed more rapid economic expansion as shown by the gross domestic product (GDP) and energy consumption statistics in Figure S1 in the supplementary information (SI).

Ten basic variables in the ECMWF dataset are considered. They include four surface-level variables: ground surface pressure (SP) in hPa, two-meter air temperature (T2M) and dew-point temperature (D2M) both in $Kelvin$ and total precipitation (PREC) in $meter$; and two variables on the intensity of turbulent processes and vertical structure of the boundary layer: boundary layer dissipation (BLD) in J/m^3 and height (BLH) in $meter$.

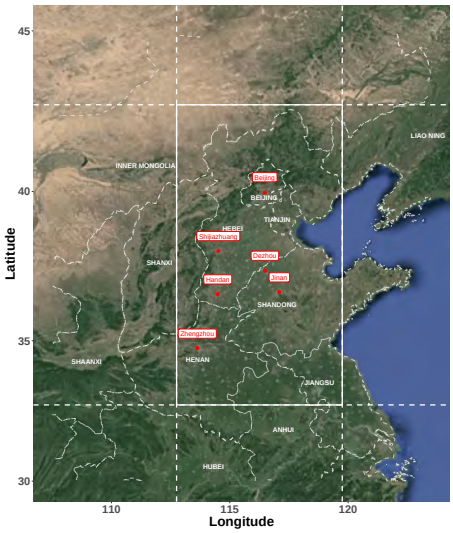

Figure 1. The study region marked within the white square (32.75° N to 42.75° N in latitude and from 112.75° E to 119.75° E in longitude excluding sea area) with the red dots marking six selected cities where we will conduct further analysis.

The choice of these variables is due to their roles in defining the basic meteorological condition within the boundary layer: the secondary generation (D2M and T2M), removal (PREC) and vertical dispersion (SP, BLH and BLD) of $PM_{2.5}$.

The remaining four variables are wind speed vector (u, v) in the eastward and northward components due to their effects on the horizontal removal or transportation of pollutants, temperature (T) in $Kelvin$ and specific humidity (SH) in $kgkg^{-1}$. The four are available over vertical pressure layers from 1000 hPa to 300 hPa, with a 25 hPa increment from 1000 to 750 hPa (11 layers) and a 50 hPa increment above 750 hPa (9 layers to 300 hPa). We did not consider data above 300 hPa as those pressure levels are well above the boundary layer in all seasons as shown in Figure S2 in the SI.

The following variables at each pressure layer are deduced from the ECMWF dataset. They include potential temperature (PT), relative humidity (RH), and wind speed WS= $\sqrt{u^2 + v^2}$. Furthermore, we categorize wind to four broad directions NE, NW, SE and SW according to NE in $[0°, 90°)$, NW in $[90°, 180°)$, SW in $[180°, 270°)$ and SE in $[270°, 360°)$. Non-zero wind speed is assigned to the prevailing wind direction at pressure level p at time t, while the other three directions' are set to zero.

As air pollution is affected by meteorological conditions at all pressure levels within the boundary layer, we integrate each variable over the pressures levels beneath the boundary layer at a time, and obtain integrated wind speed at the four directions, denoted as (INE, INW, ISE, ISW), integrated potential temperature (IPT), integrated specific humidity (ISH) and integrated relative humidity (IRH). Indeed, the cleaning or increasing effects of $PM_{2.5}$ are the act of the winds within the air column rather than at a single pressure level, which has been used in Wuerch et al. (1972), Egan and Mahoney (1972) and Holzworth (1972). Figure S2 in the SI provides distributions of the numbers of pressure layers inside the BL for each season and time of the day from the years 1979 to 2016.

The assimilated data are subject to errors as reported in Travis et al. (2016), since they depend on the quality of the models used for the underlying meteorological process. To gain information on the quality of the assimilated meteorology by ECMWF in the study region, we have computed monthly Pearson's correlation coefficients between the

assimilated surface pressure (SP), temperature (T2M) and relative humidity (RH) with the corresponding site measurements from 2010 to 2016 over 67 grid points where site observations are available. The same correlations are also computed for another assimilated data dataset, NASA's MERRA2 (Modern-Era Retrospective Analysis for Research and Applications Version 2). The correlations are displayed in Figures S3 of SI and are summarized in Tables S1 of SI. Table S1 shows that ECMWF had substantially higher correlations with the site measurements than MERRA2 in T2M (9.3% higher) and RH (55.1% higher). Although ECMWF's correlations were 5% lower than those of MERRA2 for SP, the monthly averaged correlations were all higher than 0.898. This lends support to the assimilated meteorology by ECMWF relative to MERRA2 for the study region.

2.3 Air Pollution Data

The air pollution data are $PM_{2.5}$ observations at the hourly frequency from 161 air-quality monitoring sites at 32 cities in the study region. These sites are the so-called Guokong (nationally controlled) sites, which are directly administrated by the Ministry of Ecology and Environment with the data transmitted instantaneously to a data center in Beijing to avoid potential local interference. Regional monitoring data on $PM_{2.5}$ were not available before Year 2013, the year China's air quality monitoring network was established. We did not use $PM_{2.5}$ data prior to 2014 as they endured high proportions of missing values in the study region. To match the six-hourly frequency of the meteorological data, we choose $PM_{2.5}$ data at 0200, 0800, 1200 and 2000LT. The data were available from January 2013 when China first established a national air quality monitoring network. The quality of the data was evaluated in Liang et al. (2016) in a comparative study to data from the US diplomatic posts in China, and they found the two data sources were highly consistent.

Considering the air quality data is to establish a relationship between the meteorological variables and $PM_{2.5}$ concentration so that the impact of meteorological change on air pollution can be evaluated. The air quality sites are matched to the center of the nearest grid in the ECMWF data. The locations of the 161 sites with the grids overlaid are shown in Figure S5 of SI.

2.4 Models and Assumptions

Let X denote one of the meteorological variables (SP, T2M, D2M, BLH, BLD, IPT, IRH, INW, INE, ISW and ISE), and $X_{iajt}(s)$ denote the observed value at a grid location s at Period $i \in \{1, 2\}$ (one of the two 19 year periods), year $a \in \{1, \cdots, 18\}$, month $j \in \{1, \cdots 12\}$, and a six-hourly $t \in \{1, \cdots, n_j\}$. Namely, it is the t-th observations in month j that has a total of n_j observations.

The model for the meteorological variable at a grid s is

$$X_{iajt}(s) = \mu_j^F(t; s) + \mu_{ij}^C(t; s) + \epsilon_{iajt}(s), \tag{1}$$

where $\mu_j^F(t; s)$ denotes the pre-1998 average at each time t of month j, $\mu_{ij}^C(t; s)$ represents the meteorological change term and $\epsilon_{iajt}(s)$ is the random error for natural internal variability in the system. The fixed effect $\mu_j^F(t; s)$ describes the underlying pre-1998 climatological regime and is indexed to the time t of month j, reflecting the underlying meteorological pattern at grid location s and the particular time t of the month.

The meteorological change term $\mu_{ij}^C(t; s)$ measures the change between the two 19-years periods. To make the model identifiable, we assume in Period 1

$$\mu_{1j}^C(t) \equiv 0 \quad \text{for all } j \text{ and } t.$$

Moreover, we assume the meteorological change in Period 2, if any, is time-homogeneous within a month j so that

$$\mu_{2j}^C(t) = \Delta_j. \tag{2}$$

The random errors $\{\epsilon_{iajt}(s)\}$ are serially dependent satisfying the α-mixing condition (Bosq, 1998; Fan & Yao, 2008) to reflect the temporal persistence of the meteorological processes. It is reasonable to assume

$$\begin{aligned} &\epsilon_{iajt}(s_1) \text{ and } \epsilon_{ia'jt'}(s_2) \text{ are independent for any } t \text{ and } t' \\ &\text{and any two grid locations } s_1 \text{ and } s_2 \text{ as long as } a \neq a', \end{aligned} \tag{3}$$

namely the residual series in different years are independent.

The null and alternative hypotheses we want to test for month j at grid s are, respectively,

$$H_{0js} : \mu_{2j}^C(t;s) = 0 \; versus \; H_{1js} : \mu_{2j}^C(t;s) \neq 0. \tag{4}$$

To remove the fixed effect $\mu_j^F(t;s)$, which represents the underlying meteorological pattern, we take differences between the two periods to attain

$$Y_{aj}(t;s) \hat{=} X_{2aj}(t;s) - X_{1aj}(t;s) = \mu_{2j}^C(t) + \epsilon_{2ajt}(s) - \epsilon_{1ajt}(s).$$

The test statistic for the meteorological change hypothesis (4) is

$$T_j(s) = \frac{1}{19n_j} \sum_{a=1}^{19} \sum_{t=1}^{n_j} Y_{aj}(t;s). \tag{5}$$

It can be shown that $T_j(s)$ is asymptotic normally distributed under H_{0js} such that

$$\sqrt{19n_j} T_j(s) \to N(0, \sigma_j^2(s)) \quad \text{in distribution} \quad \text{as} \quad n_j \to \infty,$$

where $\sigma_j^2(s)$ is the asymptotic variance of $T_j(s)$. As the residuals are temporally dependent, we use the spectral density approach (Brockwell & Davis, 2013; S. X. Chen & Tang, 2005) to obtain a consistent estimator $\hat{\sigma}_j(s)$ of $\sigma_j(s)$. See Appendix A.1 for more details.

2.5 Control False Discovery Rate

The proposed testing for meteorological changes over the two 19-year periods is conducted by obtaining the p-value on each grid box first followed by combining the p-values from all the 261 grid boxes with the controlled false discovery rate (FDR). Specifically, for each meteorological variable, we conduct 261 tests based on the statistics $\{T_j(s)\}_{s=1}^{261}$ that correspond to the 261 grids in the study region at each month $j = 1, \cdots 12$. Due to the repeated testing over the 261 grids, there will be an accumulation of false rejections (false discoveries), namely rejecting no-meteorological change simply due to the type-I testing error. To control the false discoveries, we carry out a multiple testing procedure that controls the FDR (Benjamini & Hochberg, 1995). Specifically, for each variable to be tested for meteorological changes between the two periods, let $\eta_1, \eta_2, ..., \eta_{261}$ be the p-values of the tests for the hypotheses H_{0js}, $s = 1, \cdots, 261$, respectively; and let $\eta_{(1)} \leq \eta_{(2)} \leq ... \leq \eta_{(m)}$ be the p-values in ascending order. The multiple testing procedure that controls the FDR at an α-level rejects all $H_{(0js)}$ with $\eta_{(i)} \leq (i\alpha)/261$. In our study, we set $\alpha = 0.05$.

It is noted that the variation in the data and the test statistic at each grid-box is assessed in the context of the 261 grid-boxes via the FDR control. The FDR control leads to smaller significance levels $(i\alpha)/261$ instead of α at the grid level, which would reduce the influence of outliers on the conclusion of the analysis.

3 Detecting Meteorological Changes from 1979 to 2016

We present testing results on statistically significant changes in the meteorological variables between the two 19-year periods from 1979 to 2016, which will be used as

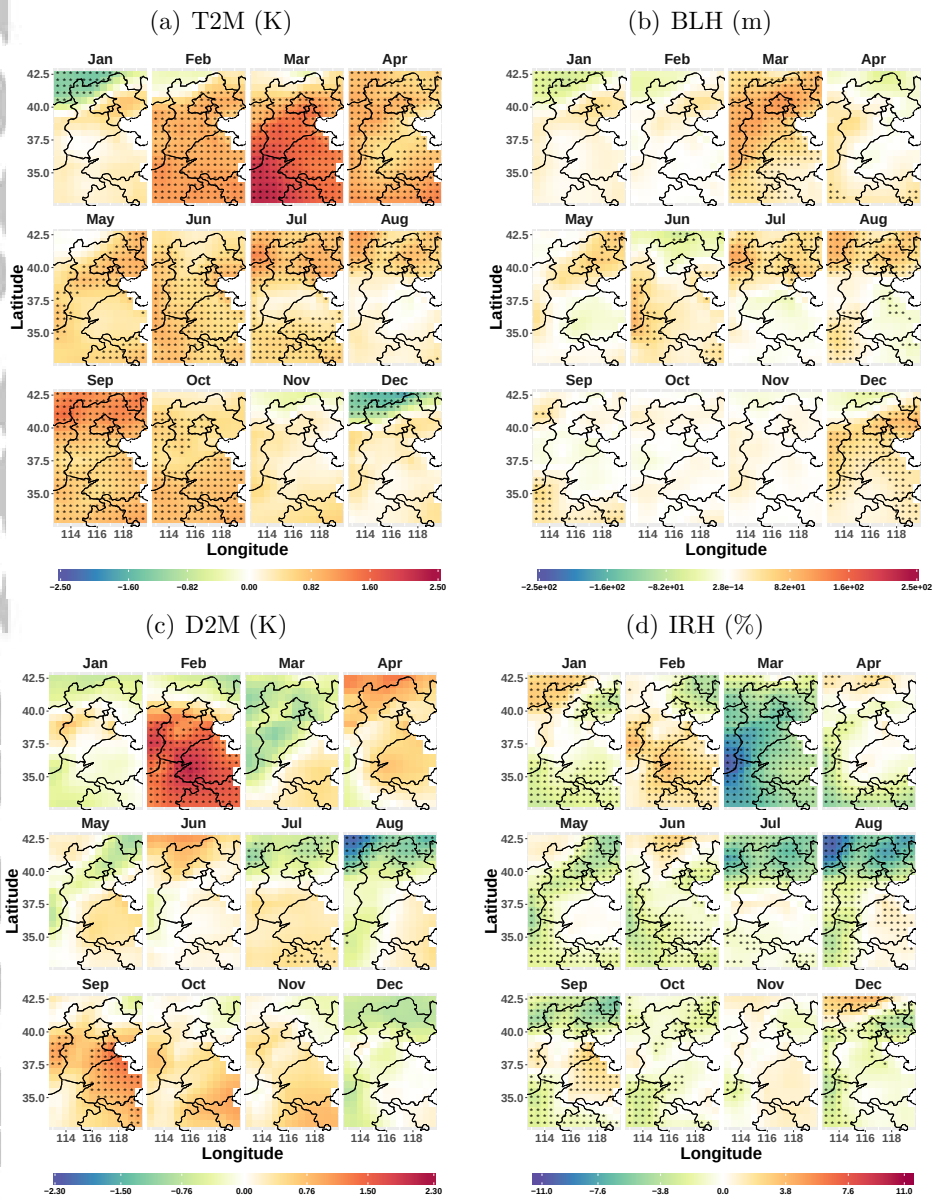

Figure 2. Differences between two 19-year periods' average values for two meter temperature (in *Kelvin*) (a), boundary layer height (BLH in meter) (b), two meter dew point temperature (in *Kelvin*) (c) and integrated relative humidity (in %) (d) for the twelve months at the 261 grids between the two time periods. Redness (blueness) indicate an increase (decrease) in a variable while stars mark statistically significance change by controlling the FDR at 5%. Black lines mark the provincial borders.

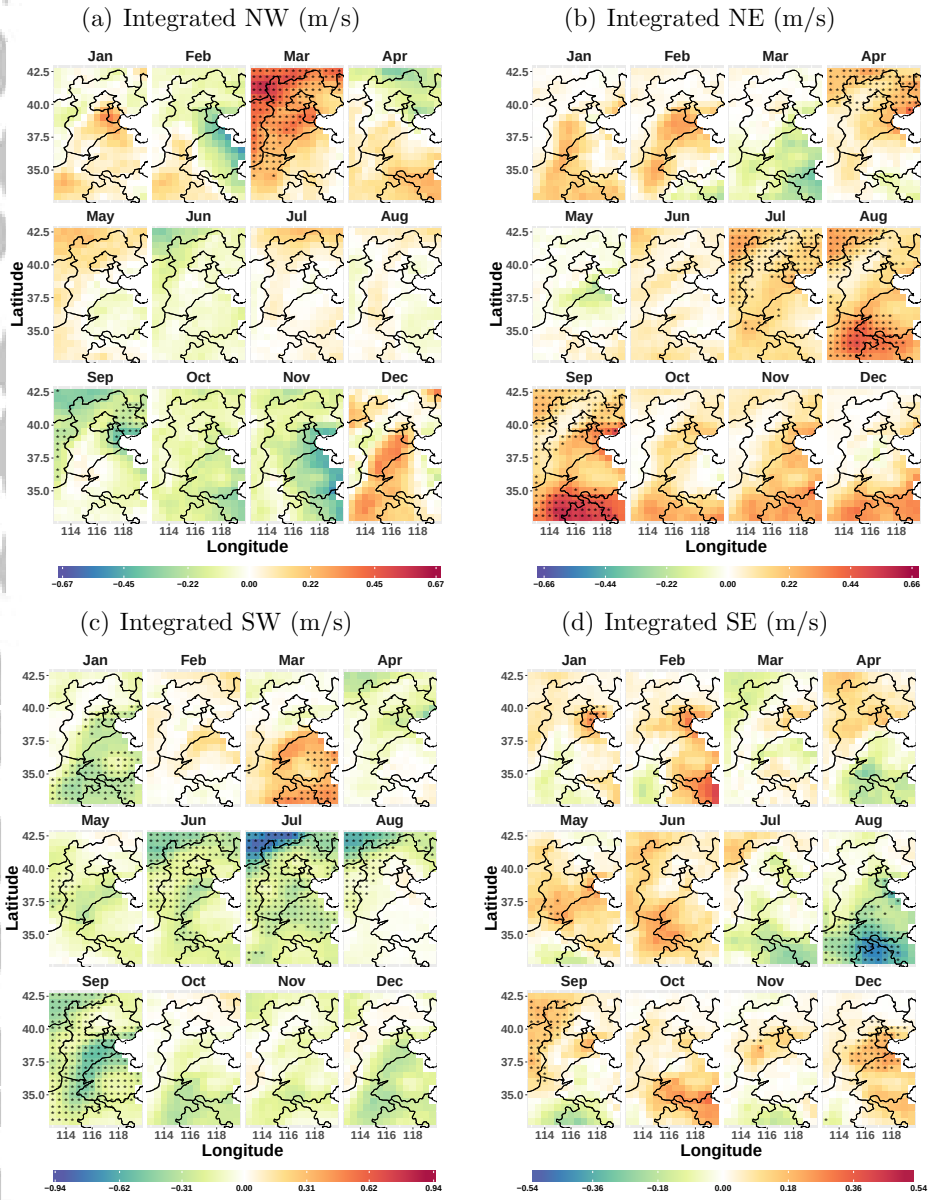

Figure 3. Differences between two 19-year periods' averages for the integrated wind speed (meter/second) at four directions: NW (a), NE (b), SW (c) and SE (d) for the twelve months at the 261 grids between the two time periods. Redness (blueness) indicate increase (decrease) in the variable while stars mark significance change by controlling the FDR at 5%.

the meteorological inputs in Section 5 when we quantify their effects on the $PM_{2.5}$ under the emission profiles of the three years from 2014 to 2016. Figure 2 displays results on T2M, BLH, D2M, and IRH for the twelve months at the 261 grids.

The most pronounced changes between the two 19-year periods were in the two-meter temperature (T2M) whose change was evident in the nine months from February to October over a large area of the study region. This confirmed surface warming over a vast portion of the region by about 0.54 K (0.2% of the average T2M in Period 1) in the nine months. There were some significant decreases for the surface temperature in the mountainous north-west corner in December and January. From November to January, decreased temperature (statistically significant or not) only occurred in northwestern mountain areas. For the vast areas in the NCP, there was no grid that had decreased T2M from November to January, and six of the nine months between February and October witnessed significant increases over 70% of the grids.

BLH was significantly increased in March at 88% of the grids, followed by December at around 50% of the grids. The average increase in March over the entire region was 57m (representing 9% of the average in Period 1), and the average increase in December was 27m (7% of the average in Period 1). BLH also increased in July and August in the northern part of the region, and it only significantly decreased in an area that consisted of 11% of the grids toward the northwest corner in January, and no more than 9 grids in June and December toward the northern edge of the region. Figure 2 indicates that the change in T2M was consistent with the change of BLH in most months because the temperature is a determining factor of BLH.

Consistent with the BLH, the average BLD in Period 2 (shown in Figure S9) had significantly increased over quite a large area (more than 50% of grids) in March and December representing 25% and 15% increase over the average in Period 1, respectively. It decreased over the north and east area of the region in June and no much change in the other nine months.

Much less average changes were detected for D2M. The two-meter dew point temperature was increased in February in a vast area south of Beijing over more than 80% of grids. D2M was lower in Period 2 at 31 and 75 grids in July and August, respectively. It is noted that the significant surface warming in Period 2 had not translated to much increase in D2M as North China became drier by a decrease in IRH as shown in panel (d) of Figure 2. This was because the warming was much canceled by the decrease in IRH that led to a rather stable dew point temperature. An increase in D2M would be bad news as it is positively correlated with $PM_{2.5}$ as shown in the next section.

The changes between the two periods for the vertically integrated potential temperature (IPT) and specific humidity (ISH), as shown in Figure S6 of SI, had similar patterns to those of T2M and D2M, respectively, which suggests that the situations within the BL are highly correlated with those at the surface level. Figure S7 also displays the changes in the precipitation (PREC), which shows that the amount of precipitation was significantly reduced as was the case for the RH in the northern part of the regions over the summer, which was part of the reason that prevented D2M to raise despite the warming.

As will be shown later on the relationship between $PM_{2.5}$ and the meteorological variables, increased BLH and BLD, and lower dew point temperature tended to reduce the level of $PM_{2.5}$. The lower dew point in the northern edge of the region (just north of Beijing) also helped reduce $PM_{2.5}$.

Figure 3 presents the average changes in the integrated wind speed in the four directions. The most significant changes occurred in the NE and SW winds, with the NE significantly increased from July to September and SW decreased from June to September over a large portion of the region. For INW and ISE, the changes were much sub-

dued. INW increased in March over a large area in the north and west part of the region and decreased in the central west and a northeast area in September. There were no significant changes in the other ten months, and especially no significant changes in three winter months. ISE decreased in the southern area of Henan province in August, and increased in Shanxi and northwest of Beijing in September and an area of eastern Hebei and Tianjin in December. The increase in December was negative news for air quality in Beijing as it led to the transportation of pollution from the heavily industrialized area south and east of Beijing.

Overall, we did not see a significant reduction in the average NW wind in the region and the area around Beijing in particular, except over two areas in September. September is a month with relatively low air pollution. The significant increase in the NE wind and the reduction in SW wind were favorable to relief the air pollution as shown in the next section. For three winter months, when the air pollution was the severest, the vertically integrated wind speeds of the four directions showed no obvious change, which suggested that the pollution in winter could not be attributed to a decrease in the northerly wind.

To justify for the choice of the 19-year bin, we have implemented the same test over a smaller temporal bin of 9 years. Specifically, we replicated the testing for meteorological changes over 9-year bins within the first and the second 19-year periods with a middle gap year, respectively, and also the changes between the second 9-year of the first 19 year period and the first 9-year of the second 19-year period. The test results are displayed in Figure S12 in the SI. When the size of the temporal bin was reduced to 9 years, more significant changes were detected which indicated more internal variability and a pattern that might differ from the pattern using the 19-year bin. This was largely due to the short term temporal variation of the data. However, by averaging over the two 19-years bins, we detected more stable meteorological changes of longer-term, which are the changes we are interested in this study.

4 Impacts of Meteorological variables on $PM_{2.5}$ in Winter

To establish a quantitative relationship between the air quality and the meteorological variables, we conduct a regression analysis that links $PM_{2.5}$ concentration with the nine meteorological variables in six major cities in the region: Beijing, Dezhou, Handan, Jinan, Shijiazhuang and Zhengzhou, which are well separated spatially as shown in Figure 1. Beijing's $PM_{2.5}$ data were from nine sites after excluding one background measurement site and two sites in the outlying northern districts. The numbers of sites for the other five cities were three in Dezhou and Handan, respectively, six in Jinan, five in Shijiazhuang and seven in Zhengzhou. As air pollution is the most severe in the winter heating season for the study region, we focus on two heating seasons from November 15, 2014/2015 to March 15, 2015/2016, respectively. Next section will consider other months of the year in all 32 cities in a larger scale analysis. Our purpose here is to build yearly meteorology to $PM_{2.5}$ profiles from 2014 to 2016, which will be used to quantify effects of the meteorological changes happened from 1979 to 2016 on 2014-2016's $PM_{2.5}$ in the next section.

Let $Y_{at}(c, s)$ be the logarithm of $PM_{2.5}$ at site s of city c, year a ($a = 1, 2$ for two heating seasons) and time t, and $X_{at}(c, s)$ consists of the nine meteorological variables: SP, logarithm of BLD (LogBLD), logarithm of BLH (LogBLH), T2M, D2M, INE, INW, ISE, ISW and lagged $PM_{2.5}$ in the previous six hours. The log-transform is to reduce the skewness in $PM_{2.5}$ and those meteorological variables to make them more symmetrically distributed. We did not include precipitation (PREC) as the region is very dry in winter, which would result in a vast number of zero values. Neither we considered IPT or IRH as they are highly correlated with T2M and D2M, respectively. The models with

D2M replaced by IRH and ISH respectively, and T2M replaced by IPT all had lower R^2's as shown in Tables S2, S4 and S5 of the SI, which lends support for the use of D2M.

The regression model is

$$Y_{at}(c,s) = \alpha_a(c) + \beta_a^T(c)X_{at}(c,s) + \gamma_a(c)Y_{a(t-1)}(c,s) + \eta_a^T(c)I_t + \epsilon_{at}(c,s), \qquad (6)$$

where $\alpha_a(c)$ represents the fixed effect in each city and $\beta_a(c)$ is the regression coefficient to the meteorological variables, $I_t \coloneqq (I_8(t), I_{14}(t), I_{20}(t))^T$ are indicators for 08:00, 14:00 and 20:00 local times respectively, $\eta_a(c)$ are the fixed time effects at the three hours, and $\epsilon_{at}(c,s)$ are residuals with zero mean and a finite variance. Specifically, $I_8(t) = 1$ when t corresponds to 08:00, and 0 otherwise; and the two other indicators $I_{14}(t)$ and $I_{20}(t)$ can be defined similarly. As the study utilizes the six-hourly data, I_t reflects the diurnal emission pattern at 08:00, 14:00 and 20:00, respectively, with that at the 02:00 being the baseline.

Model (6) has an auto-regressive (AR) component via the lagged term $\gamma_a(c)Y_{a(t-1)}(c,s)$. Auto-regressive models have been utilized in modeling the stratospheric ozone (Bojkov et al., 1990; Reinsel et al., 2005). The process of $PM_{2.5}$ consists of several major forces: the underlying emission, the meteorology as well as their interaction. If we difference Model (6) between times t and $t-1$, we attain

$$\Delta Y_{at}(c,s) = \beta_a^T(c)\Delta X_{at}(c,s) + \eta_a^T(c)\Delta I_t + \gamma_a(c)\Delta Y_{a(t-1)}(c,s) + \Delta\epsilon_{at}(c,s),$$

where Δ is the difference operator with respect to t. The difference model implies that the changes in $PM_{2.5}$ at time t is driven by a change of meteorological variable at time t and the change of $PM_{2.5}$ at the previous time $t-1$, which reflects the changes in the underlying emission in the previous time period.

Another physical interpretation of the auto-regressive Model (6) is attained if we substitute $Y_{a(t-1)}(c,s)$ by $t-1$ meteorological variables and $t-2$ pollution concentration $Y_{a(t-2)}(c,s)$ according to (6), and repeat it recursively for L times to attain

$$\begin{aligned} Y_{at}(c,s) \quad = \quad & \alpha_a(c)\sum_{l=0}^{L}\gamma_a^l(c) + \sum_{l=0}^{L}\gamma_a^l(c)[\beta_a^T(c)X_{a(t-l)}(c,s) + \eta_a^T(c)I_{t-l})] \\ & + \gamma_a^L(c)Y_{a(t-L)}(c,s) + \sum_{l=0}^{L}\gamma_a^l(c)\epsilon_{a(t-l)}(c,s). \end{aligned} \qquad (7)$$

This form implies that $PM_{2.5}$ at time t depends on a cumulative effects of the meteorological variables from times $t-L+1$ to t and the "initial" $PM_{2.5}$ value $Y_{a(t-L)}(c,s)$ at $t-L$, in the presence of the city fixed effect and the diurnal effect. The cumulative meteorological effects are transferred iteratively from the lagged $PM_{2.5}$ term.

Model (6) is a yearly-stratified model, proposed largely because emission data at the six-hourly frequency are not available and yet a much changing emission profile between years 2014 and 2016 due to the pollution mitigation initiative in the study region. A model that is based on the entire data (un-stratified) with a yearly dummy variable would still have heterogeneity due to the changing emission profiles, which cannot be fully explained by the yearly dummy variable. The impacts of the emission are reflected in the intercept parameter $\alpha_a(c)$, the three 6-hourly dummy variables and the regression coefficients $\beta_a(c)$.

In fitting the regression model, data from all monitoring sites in a city were pooled together to estimate the regression coefficients. This would alleviate to certain extent the sample size issue when fitting the yearly models. It is noted from Table 1 that despite we conducted the yearly regression, the sign and the magnitude of the significant regression coefficients over the two heating seasons in each city were largely consistent,

indicating a certain degree of model robustness. To make the estimated regression coefficients directly comparable, we standardized all meteorological variables in (6) by their respective means and standard deviations. The coefficients $\alpha_a(c)$, $\eta_a(c)$ and $\beta_a(c)$ were estimated with the ordinary least squares. The standard deviations of the estimates were obtained by the AR-Sieve bootstrap (Bühlmann, 2002), which led to the p-values for the significance of the regression coefficients.

Table 1. Estimated regression coefficients of model (6) and their statistical significance for two heating seasons of the six cities.

(a) November 15th 2014 to March 15th 2015

	Beijing	Dezhou	Handan	Jinan	SJZ	Zhengzhou
SP	-0.06***	-0.1131***	-0.036	-0.08***	-0.0102	-0.009
T2M	0.01	-0.0365	-0.003	-0.09**	0.0114	0.186***
D2M	0.08***	0.178***	0.082**	0.23***	-6e-04	-0.013
LogBLD	-0.14***	-0.1547***	-0.064*	-0.17***	-0.0121	-0.117***
LogBLH	-0.19***	-0.1737**	0.022	-0.11**	-0.1233***	0.013
INW	-0.01	0.113*	-0.124***	0.2***	-0.2029***	-0.048
INE	-0.07***	0.1244***	-0.009	0.17***	-0.0365*	-0.003
ISW	0.06***	0.0723*	-0.077**	0.09***	0.0737***	-0.049**
ISE	0.02*	0.0365	-0.01	0.08***	0.0231**	-0.05***
hour8	-0.02	0.0166	-0.212***	0.02	-0.1004***	0.062***
hour14	0.08***	2e-04***	-0.233	0.09***	-0.1913	-0.204
hour20	0.16	0.0972	-0.147	0.18**	-0.0442	0.072***
Lagged Y	0.61***	0.5474***	0.586**	0.57***	0.5724	0.682
R^2	0.66	0.60	0.49	0.55	0.60	0.64

(b) November 15th 2015 to March 15th 2016

SP	-0.058***	-0.07*	-0.09***	-0.0446**	-0.002	-0.026*
T2M	-0.034*	-0.15**	-0.19***	-0.0729**	-0.074**	0.007
D2M	0.128***	0.16**	0.15***	0.1175***	0.105***	0.025*
LogBLD	-0.077***	-0.16***	-0.06*	-0.124***	-0.002	-0.145***
LogBLH	-0.202***	-0.12**	0.08**	-0.0423	-0.11***	0.044**
INW	-0.029*	0.05	-0.35***	-0.0763**	-0.233***	-0.097***
INE	-0.039***	-0.01	-0.09***	-0.0574*	-0.097***	-0.091***
ISW	0.025**	0.06**	-0.13***	-0.0474**	0.007	-0.032**
ISE	-0.038***	0.03	-0.13***	-8e-04	-0.027***	-0.058***
hour8	0.002	0.05*	-0.05*	0.0505***	-0.113***	0.032**
hour14	0.179***	0.05*	-0.08***	0.0441**	-0.096	-0.11*
hour20	0.167*	0.11**	0.13***	0.1152**	0.095**	0.099
Lagged Y	0.644***	0.64**	0.6***	0.6928***	0.599***	0.762*
R^2	0.74	0.68	0.64	0.716	0.662	0.75

Note: *p<0.05; **p<0.01; ***p<0.001

Table 1 (a) & (b) report the estimated regression coefficients for the two heating seasons of the six cities with marked levels of significance. Table 2 provides the orders of meteorological covariables being selected in a forward selection procedure based on the Akaike Information Criterion (AIC). There is no surprise to see that the lagged $PM_{2.5}$ was the most significant variable in all cities with both the largest coefficient values and

Table 2. Variable ranks in the forward variable selection based on the AIC criterion, which denote the orders in which the variables were selected with the number on the left (right) based on the 2014-2015 (2015-2016) heating season of the six cities. A "-" indicates the selection procedure was ended before the variable, whose rank is set as 13.

	Beijing	Dezhou	Handan	Jinan	SJZ	Zhengzhou	Average Rank
Lagged Y	01, 01	01, 01	01, 01	01, 01	01, 01	01, 01	1.0, 1.0
Hour20	03, 02	06, 04	05, 04	03, 05	08, 04	08, 07	5.5, 4.3
LogBLD	04, 03	05, 03	02, 05	05, 04	−, −	05, 06	5.7, 5.7
LogBLH	08, 05	02, 02	−, 12	10, 02	06, 02	−, 02	8.7, 4.2
INW	02, 12	−, −	07, 02	07, 11	02, 03	02, 04	5.5, 7.5
Hour14	09, 06	08, −	03, 03	11,07	03, 07	03, 05	6.2, 6.8
D2M	06, 07	03, 05	06, 11	02, 03	−, 08	−, 11	7.2, 7.5
INE	05, 09	07, 05	−, 08	07, 13	05, 05	−, 03	8.3, 7.2
SP	07, 04	04, 07	09, 09	06, 10	−, −	−, 09	8.7, 8.7
Hour8	12, −	−, 09	04, 13	−, 06	04, 06	09, 10	9.2, 9.5
T2M	−, 11	−, 06	−, 10	04, 09	−, 09	04, 08	10 , 8.8
ISE	11,10	−, −	−, 06	08, 08	09, 10	06, 08	10 , 9.2
ISW	10,08	−, 10	08, 07	09, 12	07, −	07, 12	9.0, 10.3

the leading rank being selected, as it reflected the strong temporal persistence nature of $PM_{2.5}$. It is noted that as all the covariables had been standardized by their respective means and standard deviation, the magnitude of the estimated regression coefficients in Table 1 (a) & (b) and the ranking in Table 2 were highly consistent to each other in that those variables with larger and significant estimated coefficients (in absolute value) tended to rank higher in Table 2. The diurnal effect was significant in all six cities with at least one (two) significant hour in 2015 (2016) heating season, relative to the baseline 02:00, which also showed an increased diurnal effect between the two heating seasons.

As shown in Table 1 (a) & (b), both BLD and BLH were the top-ranked meteorological variables as reflected by both the numeric size of the estimated coefficients, the range of the p-values and the rank being selected (Table 2). The largely negative coefficients to BLD and BLH indicated their reducing effects as both variables reflect the vertical ventilation. INW ranked next in Table 2, which also had significant reducing effects on $PM_{2.5}$ in 7 out of 12 heating season and city combinations. INE had the same reducing effects, while the ranking was lower than INW. These largely confirmed the benefits of the northerly wind in the study region.

Among the three surface variables (T2M, D2M and SP), D2M was the most significant (at 5% level) in 10 out of the 12 city and season combinations with a significant $PM_{2.5}$ enhancing effect, followed by SP which had a significant reducing effect in 8 out the 12 season and city combinations. T2M had a mixed and weaker effect on $PM_{2.5}$. This was because T2M is positively correlated with both dew point temperature and BLH. However, the dew point was $PM_{2.5}$ enhancing while BLH was $PM_{2.5}$ reducing, as respectively shown by the signs of the regression coefficients in Table 1. These conflicting effects as well as the added diurnal effects via the time dummy variables made the net effect of T2M mixed and weaker.

Regarding the four integrated wind speeds, the ones at the NW and NE directions were more influential than those at SE and SW. INW and INE significantly reduced $PM_{2.5}$

in Beijing and Shijiazhuang with relatively larger coefficients and smaller p-values. The signs of the coefficients to the integrated wind speeds of the four directions reflected the geographical emission profiles surrounding a city. It is noted that INW and INE's coefficients were positive for Dezhou and Jinan in 2015 because the two cities are located south of Hebei with heavy industrial emission, and therefore, the northerly wind would bring in transported pollution. For the same reason, coefficients to the two southerly winds had more positive signs than the two northerly winds, which was especially the case for Beijing, Dezhou, and Shijiazhuang. The three cities had more sources of emission to their south. Furthermore, from Table 1 (a) & (b), we can find that except for the integrated wind speeds, nearly all the regression coefficients of the meteorological variables had stable signs between the two winter heating seasons, which implied that those variables' impacts on the air pollution were largely stable over time. Figures S7 and S8 in SI display the pairwise regressions between $PM_{2.5}$ and the meteorological variables without the lagged $PM_{2.5}$ term, whose coefficients largely had the same signs as those in Table 1 with the lagged term.

5 Meteorological Change's Effects on $PM_{2.5}$

We evaluate the effects of the meteorological change between the two 19-year periods from 1979 to 2016 on $PM_{2.5}$ under three-yearly emission regimes from 2014 to 2016, respectively. This is carried out by a two-step procedure. It first builds the regression function between $PM_{2.5}$ and the meteorological variables via Model (6) for each season (not just the heating season) of the three years from 2014 to 2016, respectively. Then, the monthly averages of the meteorological variables in the two 19-year periods are substituted, respectively, to the estimated regression functions to attain a pair of the fitted values, and their differences at each month of 2014 to 2016. The differences are the effects of the meteorological change that happened between 1979 and 2016 on $PM_{2.5}$ under the emission regimes from 2014 to 2016, respectively.

It is also noted that the three years' $PM_{2.5}$ and meteorological data from 2014 to 2016 were for establishing the relationship between $PM_{2.5}$ and the meteorological variables, rather than the meteorological changes as the latter were assessed based on 38 year's ECMWF data from 1979 to 2016.

The rationale of our method has similarity to other studies (H. Wang et al., 2015; Shen et al., 2018; Leung et al., 2018) for the climate change effects on air pollution, which are usually consists of four steps: (i) meteorology and PM correlation/regression modeling, (ii) scenarios of future climate change, (iii) scenarios of emission, (iv) obtaining the climate change effects on air pollution by substituting the climate change and emission scenarios under (ii) and (iii) to the established model in (i). The analogues of our approach to the existing approaches are in (i) we use the three year's data (2014-2016) to obtain the meteorology to pollution's models; in (ii) we use the meteorological changes observed between the two 19-year periods from the 38-year's ECMWF reanalysis data as the meteorological change scenario. However, the regression models built in (i) also served as the emission scenarios for 2014-2016 in (iii) to attain the study objective. Therefore, in (iv), we only substitute the meteorological changes attained in (ii) to the regression model in (i).

Comparing with the regression analysis in the last section, the analysis is extended beyond the six cities and the heating seasons to the 32 cities that we have air quality data and the entire year, respectively. Since most air quality sites are located in the center of a city, we match each city to one grid which is nearest to the city center, and use the grid's reanalysis data as the meteorological variables in the regression analysis for the city.

The regression model (6) that measures the meteorological effect on $PM_{2.5}$ is estimated on four seasons: (i) Heating season (q = 1): November 15th last year to March 15th, (ii) Spring (q = 2): March 16th to May 31st; (iii) Summer (q = 3): June 1st to August 31st and (iv) Fall (q = 4): September 1st to November 14th. Having the regression model built over the four seasons instead of each month is to allow enough data since we work on six-hourly instead of hourly observations.

The regression model (6) is re-expressed as

$$\begin{aligned} Y_{aqt}(c,s) &= \alpha_{aq}(c) + \beta_{aq}^T(c)X_{aqt}(c) + \gamma_{aq}(c)Y_{aq(t-1)}(c,s) \\ &\quad +\eta_{aq}^T(c)I_t + \epsilon_{aqt}(c,s), \end{aligned} \tag{8}$$

where $a = 2014, 2015$ and 2016 for the three years, $q = 1, 2, 3$ and 4 for the four seasons, and t is still the 6-hourly index, and s denotes a site in city c. The model is fitted using the same approach as that for model (6).

Let $\bar{X}_{1j}(c)$ and $\bar{X}_{2j}(c)$ be the empirical averages of the meteorological variables for month j at a city c in the two 19-years periods, respectively. The estimated effects of meteorological change on $\log(PM_{2.5})$ at month j of year a are

$$\hat{\beta}_{aq}^T(c)(\bar{X}_{2j}(c) - \bar{X}_{1j}(c))/\{1 - \hat{\gamma}_{aq}(c)\}, \tag{9}$$

where $\hat{\beta}_{aq}(c)$ and $\hat{\gamma}_{aq}(c)$ are the estimated regression coefficients for the q-th quarter that covers month j. The division of $(1-\hat{\gamma}_{aq}(c))$ is due to the iterative lagged effect by assigning $L = \infty$ in (7). Hence, the meteorological effect is accumulated like a geometric progression which results in the factor $(1-\hat{\gamma}_{aq}(c))^{-1}$ in (9). It is noted that as the effect is measured for each year from 2014 to 2016, as there is no need to pool with other year's data. The uncertainty associated with the relative small sample size is alleviated as we merge the multiple air quality monitoring sites in each city, which allows more data in building the yearly regression model in the paper. It is noted that the air quality sites in a city are close to each other relative to the size of the grid boxes for the ECMWF reanalysis data, which supports the site merge.

We transform the meteorological effects on log $PM_{2.5}$ back to $PM_{2.5}$ by the exponential transform to attain $\hat{\nu}_{2aj}(c) - \hat{\nu}_{1aj}(c)$ where $\hat{\nu}_{iaj}(c) = \exp\{(\hat{\alpha}_{aq}^T(c) + \hat{\beta}_{aq}^T(c)\bar{X}_{ij}(c) + \hat{\eta}_{aq}^T(c)\bar{I})/(1 - \hat{\gamma}_{aq}(c))\}$ is the average $PM_{2.5}$ (in $\mu g/m^3$) at month j of year a in a city c, and $\bar{I} = (0.25, 0.25, 0.25)^T$ is the average indicator values over the two periods. The standard errors can be obtained as outlined in Appendix A.2. For March and November, we average the effects for $q = 1$ and 2, and $q = 1$ and 4, respectively, since March (November) falls to heating ($q = 4$) and the spring (fall) seasons, respectively.

Figure 4 presents the monthly meteorological change effects on $PM_{2.5}$ for each city, which displays significant decreases in $PM_{2.5}$ in January, March, and December in all three years from 2014 to 2016. November was the only month that had increased $PM_{2.5}$ in some cities.

Figure 5 aggregates the results in Figure 4 by providing the raw and relative meteorological change effects for each month on $PM_{2.5}$. It shows that the overall effects of the meteorological change in the 32 cities were largely consistent among the three years. Figure 5 (a) shows that the percentages of cities that experienced unfavorable effects (increased $PM_{2.5}$) were far less than those with favorable effects (reducing $PM_{2.5}$). In particular, the percentages of favorable effects were all above 47% in January, March and December across the three years. June was the month that had the largest unfavorable percentage changes at 11.6% on average, followed by November. The confidence intervals given in panel (b) shows that the unfavorable effects in June and November were not significant at the 5% level. In contrast, the favorable effects in January, March, and December implicated in Figure 4 were confirmed at 5% level of significance. There was evidence of the favorable effects of the meteorological changes on $PM_{2.5}$ in the five months

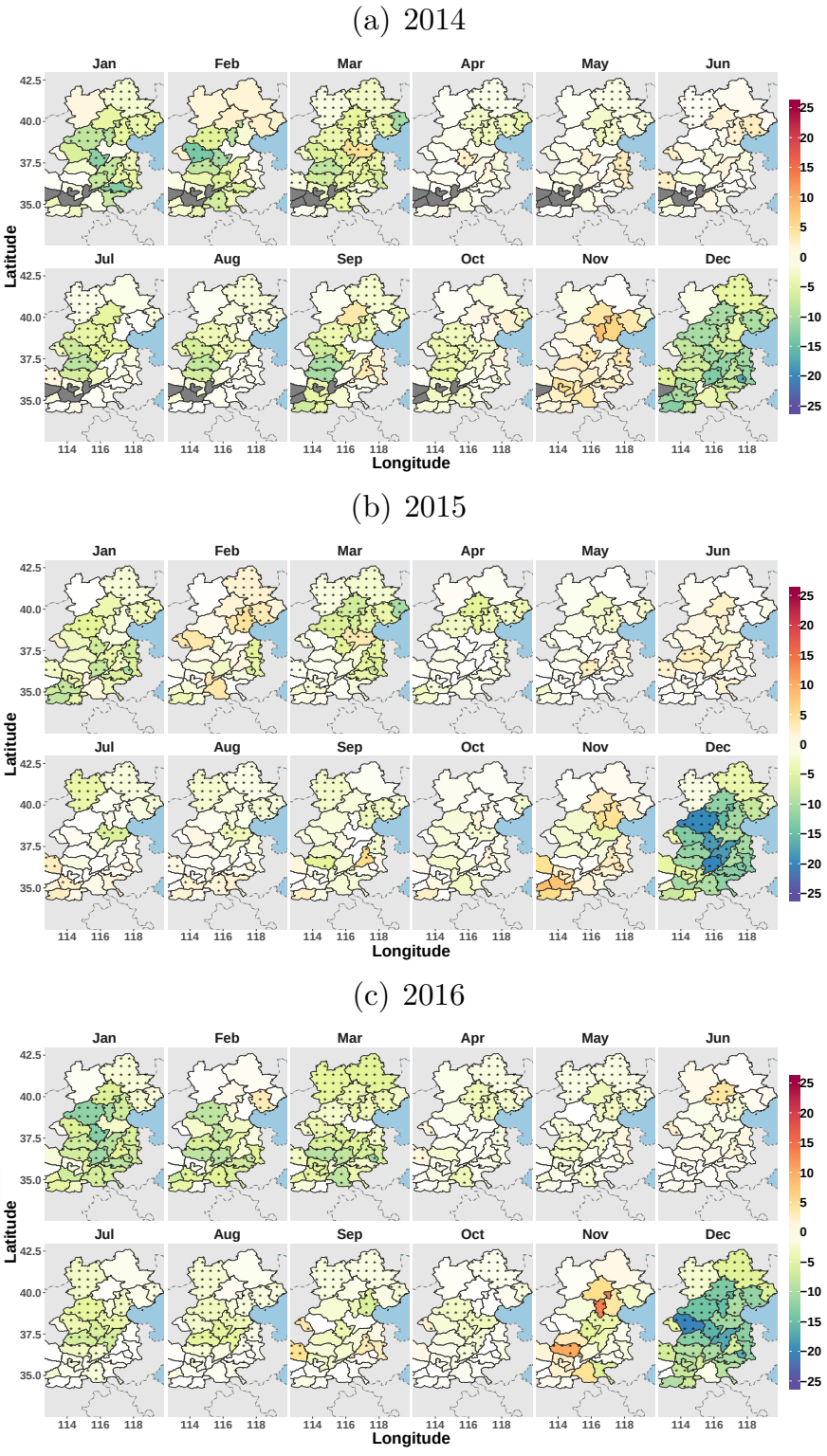

Figure 4. Estimated meteorological change effects on $PM_{2.5}$ (in $\mu g/m^3$) for the 32 cities . The effects are shown for the twelve months between years of 2014 and 2016. We mark all the grids with stars for cities with significant changes (at 5% level). (In 2014, some cities are missing because of the high data missing rate in the sites.)

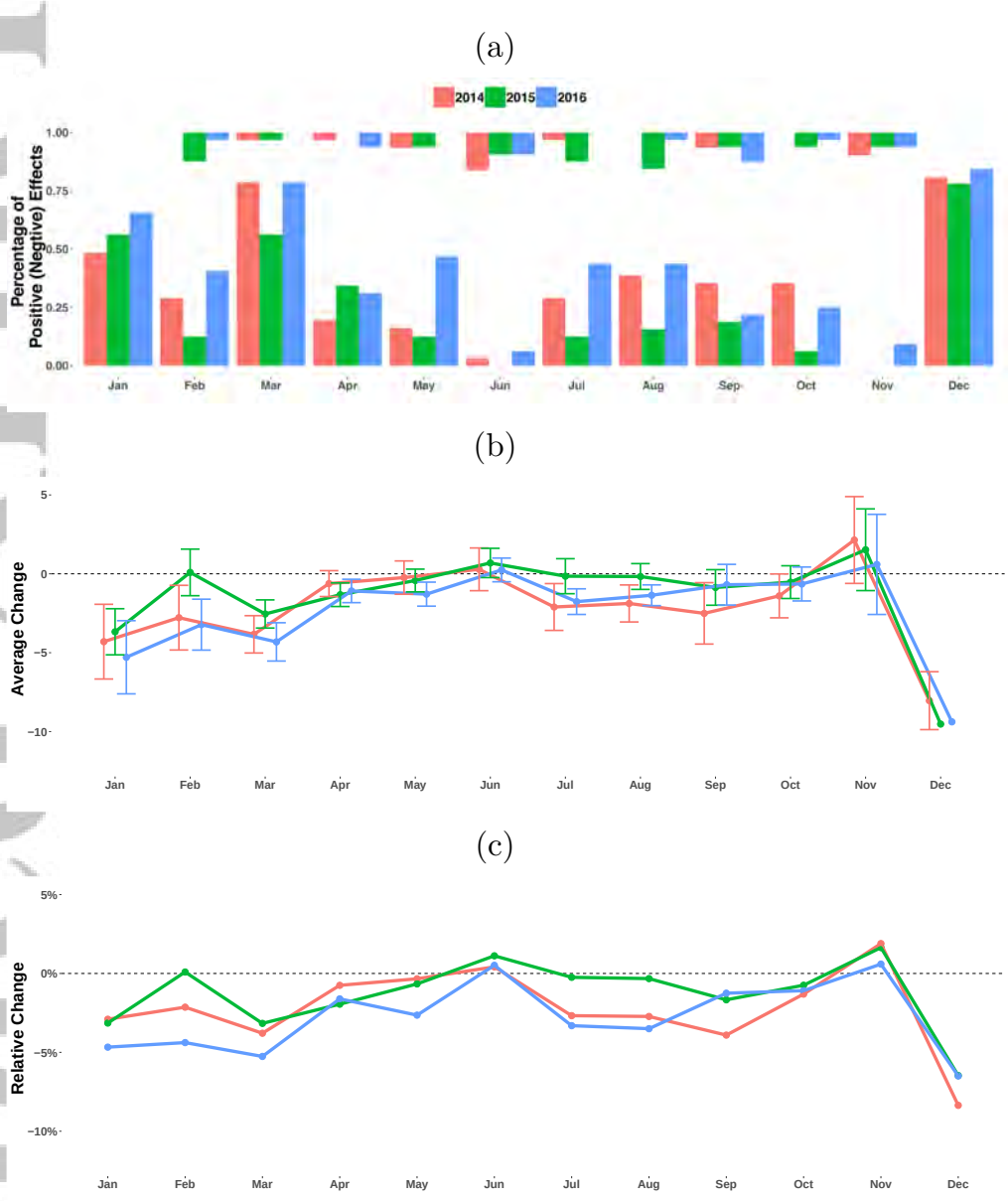

Figure 5. Percentages of cities that had significant meteorological change effects (a), and the absolute (b) and relative (c) (related to original average) average $PM_{2.5}$ changes (in $\mu g/m^3$) in the 32 cities in the three years. In (a), bars from bottom (top) indicate percentages of the cities which had significant favorable (unfavorable) meteorological change effects on $PM_{2.5}$; (b), the average meteorological change effects and the 95% confidence intervals over all 32 cities; (c), relative meteorological change effects over the 32 cities.

of April, July, August, September, and October, where the overall estimated regional effects were negative. Among the 15 month-year combinations, there were 8 of them being statistically significant at 5% level and the other 7 were not significant. But, still, we can see the quite strong evidence of the favorable effects of the meteorological changes.

The months of January, March, and December experienced the most favorable and significant meteorological effects with the average $PM_{2.5}$ reduced between $2.55 \sim 9.52$ $\mu g/m^3$. The amount of reduction in January and December, the two worst months for air quality, amounted to about 3.57% and 7.10% of the average $PM_{2.5}$, respectively and were highly significant. Despite the meteorological change effect were significant statistically, the average annual percentages of reduction for 2014-2016's $PM_{2.5}$ ranged from 1.29% to 2.76% that mounted to $1.41 \sim 2.35$ $\mu g/m^3$ reduction per year. Thus, they accounted for only a small percentage of $PM_{2.5}$ concentration as shown in Figure 5 (c), which means that the alleviating effects of the meteorological change were rather limited and could not be relied upon for solving the air pollution problem in the region.

6 Discussion

The observed percentage range of effects due to the meteorological change was consistent with some existing studies. Tagaris et al. (2007) projected continental US's annual average $PM_{2.5}$ concentration to decline 10% in 2050 vs the 2000 level, and Avise et al. (2009) projected the US July average $PM_{2.5}$ to be down -1$\mu g/m^3$ over the same time frame as Tagaris et al. Our results showing some limited amount of meteorological "benefit" on $PM_{2.5}$ levels in 2014-2016 were comparable with the results of Shen et al. (2018); Leung et al. (2018) and Pendergrass et al. (2019) on the climate change effects on future Beijing or eastern China's $PM_{2.5}$ level under various climate change and emission scenarios.

Our study differs from existing studies on the meteorological change's effects on air pollution in several aspects. One is that our study is based on the historical data without a need for providing explicit scenarios in emission and meteorological changes. Our study implicitly utilized emission information in the years from 2014 to 2016, and explicitly the meteorological change information from 1979 to 2016. The second difference is that our study region is much smaller spatially than some of the studies which allows us to better control hidden spatial effects shared in the region.

Our analysis reveals that the region in North China during the 38 years between 1979 and 2016 had witnessed significant changes in several meteorological variables, which include an increased surface temperature by 0.57 degree, the boundary layer height and dissipation, and the vertically integrated NE wind speed; reduced RH and vertically integrated SW wind speed. Overall speaking, the region has become warmer and dryer. The warming has led to increases in both boundary layer height and dissipation, which are the two main drivers for the favorable effect on $PM_{2.5}$. Our analysis did not confirm the widespread speculation of reduced northerly wind. In contrast, the NE wind had increased while NW wind had no sustained trend. Hence, the speculation was very much caused by increased public anxiety on air pollution as people's expectation for its improvement had increased.

The overall effects of the meteorological change had contributed to net reductions of $PM_{2.5}$ in many months of the three years after controlling for emission at each grid and month in the study region. It is noted that despite the warming, dew point temperature had been largely kept under control as the region had got dryer. This made the effects of temperature warming largely favorable to $PM_{2.5}$ as it enhances boundary layer height and dissipation. A conclusion from the analysis is that the meteorological change in North China had helped alleviate the air pollution, and was certainly not responsible for the regional air pollution problem.

Acknowledgments

The research was partially supported by China's National Key Research Special Program Grant no. 2016YFC0207701, National Natural Science Foundation of China key Grant 71532001, Center for Statistical Science and LMEQF at Peking University. The ERA-Interim reanalysis data used in this study were collected from the ECMWF website `https://apps.ecmwf.int/`. The MERRA2 dataset can be accessible at `https://gmao.gsfc.nasa.gov/reanalysis/MERRA-2/data_access/`. We archived our pollution data in the repository `https://archive.ics.uci.edu/ml/datasets/Beijing+Multi-Site+Air-Quality+Data`. A temporary copy of the data was in SI.

References

Avise, J., Chen, J., Lamb, B., Wiedinmyer, C., Guenther, A., Salathé, E., & Mass, C. (2009). Attribution of projected changes in summertime us ozone and PM 2.5 concentrations to global changes. *Atmospheric Chemistry and Physics*, *9*(4), 1111–1124. doi: https://doi.org/10.5194/acp-9-1111-2009

Benjamini, Y., & Hochberg, Y. (1995). Controlling the false discovery rate: a practical and powerful approach to multiple testing. *Journal of the Royal Statistical Society. Series B*, *57*(1), 289–300.

Bojkov, R., Bishop, L., Hill, W., Reinsel, G., & Tiao, G. (1990). A statistical trend analysis of revised Dobson total ozone data over the northern hemisphere. *Journal of Geophysical Research: Atmospheres*, *95*(D7), 9785–9807. doi: https://doi.org/10.1029/JD095iD07p09785

Bosq, D. (1998). *Nonparametric statistics for stochastic processes: estimation and prediction* (Vol. 110). New York, NY: Springer Science.

Brockwell, P. J., & Davis, R. A. (2013). *Time series: Theory and methods*. New York, NY: Springer Science & Business Media. doi: https://doi.org/10.1007/978-1-4419-0320-4

Bühlmann, P. (2002). Bootstraps for time series. *Statistical Science*, *17*(1), 52–72.

Cai, W., Li, K., Liao, H., Wang, H., & Wu, L. (2017). Weather conditions conducive to Beijing severe haze more frequent under climate change. *Nature Climate Change*, *7*(4), 257.

Chen, H., & Wang, H. (2015). Haze days in North China and the associated atmospheric circulations based on daily visibility data from 1960 to 2012. *Journal of Geophysical Research: Atmospheres*, *120*(12), 5895–5909. doi: https://doi.org/10.1002/2015JD023225

Chen, L., Guo, B., Huang, J., He, J., Wang, H., Zhang, S., & Chen, S. X. (2018). Assessing air-quality in beijing-tianjin-hebei region: The method and mixed tales of pm2. 5 and o3. *Atmospheric environment*, *193*, 290–301.

Chen, R., Zhao, Z., & Kan, H. (2013). Heavy smog and hospital visits in beijing, china. *American journal of respiratory and critical care medicine*, *188*(9), 1170–1171.

Chen, S. X., & Tang, C. (2005). Nonparametric inference of value-at-risk for dependent financial returns. *Journal of Financial Econometrics*, *3*(2), 227–255. doi: https://doi.org/10.1093/jjfinec/nbi012

Cheng, M. (2016). Beijing haze is rooted in wind attenuation (in Chinese). *China ScienceNet*. Retrieved from `http://news.sciencenet.cn`

Dee, D. P., Uppala, S., Simmons, A., Berrisford, P., Poli, P., Kobayashi, S., ... Bauer, P. (2011). The era-interim reanalysis: configuration and performance of the data assimilation system. *Quarterly Journal of the Royal Meteorological Society*, *137*(656), 553–597. doi: https://doi.org/10.1002/qj.828

Donaldson, K., Li, X., & MacNee, W. (1998). Ultrafine (nanometre) particle mediated lung injury. *Journal of aerosol science*, *29*(5-6), 553–560.

Egan, B. A., & Mahoney, J. R. (1972). Numerical modeling of advection and diffusion of urban area source pollutants. *Journal of Applied Meteorology*, *11*(2),

312–322. doi: https://doi.org/10.1175/1520-0450(1972)011⟨0312:NMOAAD⟩2.0.CO;2

Fan, J., & Yao, Q. (2008). *Nonlinear time series: Nonparametric and parametric methods*. New York, NY: Springer-Verlag.

Holzworth, G. C. (1972). Mixing heights, wind speeds, and potential for urban air pollution throughout the contiguous United States. In *United states environmental protection agency publication* (Vol. 101, p. 118). Research Triangle Park, NC: Environmental Protection Agency.

Jacob, D. J., & Winner, D. A. (2009). Effect of climate change on air quality. *Atmospheric Environment*, *43*(1), 51–63. doi: https://doi.org/10.1016/j.atmosenv.2008.09.051

Küunsch, H. R. (1989). The jackknife and the bootstrap for general stationary observations. *The Annals of Statistics*, *17*(3), 1217–1241.

Leung, D. M., Tai, A. P., Mickley, L. J., Moch, J. M., Donkelaar, A. v., Shen, L., & Martin, R. V. (2018). Synoptic meteorological modes of variability for fine particulate matter (pm 2.5) air quality in major metropolitan regions of china. *Atmospheric Chemistry and Physics*, *18*(9), 6733–6748.

Liang, X., Li, S., Zhang, S., Huang, H., & Chen, S. X. (2016). PM2.5 data reliability, consistency, and air quality assessment in five Chinese cities. *Journal of Geophysical Research: Atmospheres*, *121*, 10,220-10,236. doi: https://doi.org/10.1002/2016JD024877

Liang, X., Zou, T., Guo, B., Li, S., Zhang, H., Zhang, S., ... Chen, S. X. (2015). Assessing Beijing's PM2.5 pollution: severity, weather impact, APEC and winter heating. *Proceedings of the Royal Society A*, *471*, 20150257. doi: https://doi.org/10.1098/rspa.2015.0257

Long, X., Bei, N., Wu, J., Li, X., Tian, F., Li, X., ... An, Z. (2018). Does afforestation deteriorate haze pollution in Beijing–Tianjin–Hebei (BTH), China? *Atmospheric Chemistry and Physics*, *18*(15), 10869. doi: https://doi.org/10.5194/acp-18-10869-2018

Miao, Y., Hu, X., Liu, S., Qian, T., Xue, M., Zheng, Y., & Wang, S. (2015). Seasonal variation of local atmospheric circulations and boundary layer structure in the Beijing-Tianjin-Hebei region and implications for air quality. *Journal of Advances in Modeling Earth Systems*, *7*(4), 1602–1626. doi: https://doi.org/10.1002/2015MS000522

Pendergrass, D., Shen, L., Jacob, D., & Mickley, L. (2019). Predicting the impact of climate change on severe wintertime particulate pollution events in beijing using extreme value theory. *Geophysical Research Letters*, *46*(3), 1824–1830.

Pope III, C. A., Burnett, R. T., Thun, M. J., Calle, E. E., Krewski, D., Ito, K., & Thurston, G. D. (2002). Lung cancer, cardiopulmonary mortality, and long-term exposure to fine particulate air pollution. *Jama*, *287*(9), 1132–1141.

Reinsel, G. C., Miller, A. J., Weatherhead, E. C., Flynn, L. E., Nagatani, R. M., Tiao, G. C., & Wuebbles, D. J. (2005). Trend analysis of total ozone data for turnaround and dynamical contributions. *Journal of Geophysical Research: Atmospheres*, *110*(D16), 306. doi: https://doi.org/10.1029/2004JD004662

Schwartz, J. (2000). The distributed lag between air pollution and daily deaths. *Epidemiology*, *11*(3), 320–326.

Shen, L., Jacob, D. J., Mickley, L. J., Wang, Y., & Zhang, Q. (2018). Insignificant effect of climate change on winter haze pollution in beijing. *Atmospheric Chemistry and Physics*, *18*(23), 17489–17496.

Tagaris, E., Manomaiphiboon, K., Liao, K.-J., Leung, L. R., Woo, J.-H., He, S., ... Russell, A. G. (2007). Impacts of global climate change and emissions on regional ozone and fine particulate matter concentrations over the United States. *Journal of Geophysical Research: Atmospheres*, *112*(D14), 312. doi: https://doi.org/10.1029/2006JD008262

Tai, A. P., Mickley, L. J., & Jacob, D. J. (2010). Correlations between fine

particulate matter (PM2.5) and meteorological variables in the United States: Implications for the sensitivity of PM2.5 to climate change. *Atmospheric Environment*, *44*(32), 3976–3984. doi: https://doi.org/10.1016/j.atmosenv.2010.06.060

Tai, A. P., Mickley, L. J., Jacob, D. J., Leibensperger, E., Zhang, L., Fisher, J. A., & Pye, H. (2012). Meteorological modes of variability for fine particulate matter (PM2.5) air quality in the United States: implications for PM2.5 sensitivity to climate change. *Atmospheric Chemistry and Physics*, *12*(6), 3131–3145. doi: https://doi.org/10.5194/acp-12-3131-2012

Taylor, K. E., Stouffer, R. J., & Meehl, G. A. (2012). An overview of CMIP5 and the experiment design. *Bulletin of the American Meteorological Society*, *93*(4), 485–498. doi: https://doi.org/10.1175/BAMS-D-11-00094.1

Travis, K. R., Jacob, D. J., Fisher, J. A., Kim, P. S., Marais, E. A., Zhu, L., ... Sulprizio, M. P. (2016). Why do models overestimate surface ozone in the southeast United States ? *Atmospheric Chemistry and Physics*, *16*(21), 13561–13577. doi: https://doi.org/10.5194/acp-16-13561-2016

Wang, H., Chen, H., & Liu, J. (2015). Arctic sea ice decline intensified haze pollution in eastern china. *Atmospheric and Oceanic Science Letters*, *8*(1), 1–9.

Wang, X., Wu, J., Chen, M., Xu, X., Wang, Z., Wang, B., ... Miao, G. (2018). Field evidences for the positive effects of aerosols on tree growth. *Global Change Biology*, *24*(10), 4983–4992. doi: https://doi.org/10.1111/gcb.14339

Wuerch, D., Courtois, A., Ewald, C., & Ernct, G. (1972). A preliminary transport wind and mixing height climatology for St. Louis, Missouri. *National Oceanic and Atmospheric Administration Technical Memorandum National Weather Service Central Region*, *49*, 13.

Xu, P., Chen, Y., & Ye, X. (2013). Haze, air pollution, and health in China. *The Lancet*, *382*(9910), 2067. doi: https://doi.org/10.1016/S0140-6736(13)62693-8

Yan, L. (2015). Influence of wind power development on the heavy haze in Beijing, Tianjin and Hebei (in Chinese). *Environmental Protection and Circular Economy*(2015.09), 67–71.

Yin, Z., & Wang, H. (2016). The relationship between the subtropical western pacific sst and haze over north-central north china plain. *International Journal of Climatology*, *36*(10), 3479–3491.

Yin, Z., & Wang, H. (2017). Role of atmospheric circulations in haze pollution in december 2016. *Atmospheric Chemistry and Physics*, *17*(18), 11673.

Zhang, S., Guo, B., Dong, A., He, J., Xu, Z., & Chen, S. X. (2017). Cautionary tales on air-quality improvement in Beijing. *Proceedings of the Royal Society A: Mathematical, Physical and Engineering Sciences*, *473*, 20170457. doi: https://dx.doi.org/10.6084/m9.figshare.c.3865483

Zheng, G., Duan, F., Su, H., Ma, Y., Cheng, Y., Zheng, B., ... Chang, D. (2015). Exploring the severe winter haze in Beijing: the impact of synoptic weather, regional transport and heterogeneous reactions. *Atmospheric Chemistry and Physics*, *15*(6), 2969–2983. doi: https://doi.org/10.1175/2010JCLI3850.1

Appendix A Methods

A1 Variance Estimation for Average Climate Change.

Let $Y_{ajt}(s) = X_{2ajt}(s) - X_{1ajt}(s)$ be the difference of meteorological observations between two period in a-th year at month j and hour t at a grid s. To simplify the expedition, as the same procedures will be replicated for each year, month and grid, we will hide the subscripts a, j and s in $Y_{ajt}(s)$ and simply write it as Y_t.

Let μ be the mean of Y_t. An estimator of μ is $\hat{\mu} = n^{-1}\sum_{t=1}^{n} Y_t$, where n is the number of observations at the month. The variance is $\mathrm{Var}(\hat{\mu}) = n^{-1}\sigma^2(n)$, where $\sigma^2(n) =$

$\gamma(0)+2\sum_{k=1}^{n-1}(1-k/n)\gamma(k)\}$ and $\gamma(k)=\text{cov}(Y_t,Y_{t+k})$ for positive integers k. A common approach for variance estimation in time series is the spectral approach.

Let $\phi(\lambda)=(2\pi)^{-1}\sum_{k=-\infty}^{\infty}\gamma(k)\exp(-ik\lambda)$ for $\lambda\in[-\pi,\pi]$ be the spectral density of $\{Y_t\}_{t=1}^n$. According to (Brockwell & Davis, 2013) (Corollary 4.3.2), we can estimate $\sigma^2(n)$ with estimating $\phi(0)$.

Let $I_n(w_j)=n^{-1}|\sum_{l=1}^n Y_l e^{-ilw_j}|^2, j=0,\pm1,\cdots,\pm[n/2]$ be the sample periodogram. According to Theorem 5.2.6 of (Brockwell & Davis, 2013) for any $j\in T$

$$I_n(\omega_j)=(2\pi)\phi(\omega_j)E_j+R_j,$$

where $\{E_j\}_{j\in T}$ are independent standard exponential random variables and $\{R_j\}_{j\in T}$ are asymptotically negligible terms.

Take the logarithm on both side of equation above and ignore $\{R_j\}$

$$\log\{I_n(\omega_j)/2\pi\}=\log\{\phi(\omega_j)\}+\log(E_j)\quad j\in T. \tag{A1}$$

Note that $E\{\log(E_j)\}=-0.5$, let $\eta_j=\log(E_j)+0.57721$, $W_j=\log\{I_n(\omega_j)/2\pi\}+0.57721$. The equation (A1) can be approximated by the following nonparametric regression:

$$W_j=m(\omega_j)+\eta_j\quad j\in T.$$

The Nadaraya-Waston estimator of $m(\omega)$ based on a kernel K and a smoothing bandwidth b is

$$\hat{m}_b(\omega)=\frac{\sum_{j\in T}K_1(\frac{\omega-\omega_j}{b})W_j}{\sum_{j\in T}K_1(\frac{\omega-\omega_j}{b})}.$$

Hence, the kernel estimator of $\phi(0)$ is $\hat{\phi}(0)=\exp\{\hat{m}_b(0)\}$. The standard deviation of $\hat{\mu}$ is $2\pi\hat{\phi}(0)/n$. See (S. X. Chen & Tang, 2005) for more details.

A2 Average Climate Condition of a City

We choose the nearest grid to the average latitude and longitude of all the air quality sites in a city c to represent average meteorological condition of the city. Let $\mu_{1j}(c)$ and $\mu_{2j}(c)$ be the means of the nine dimensional vector of the meteorological variables for each month (j) for city c in the two 19-year periods, respectively. They are estimated by

$$\hat{\mu}_{lj}(c)=\frac{1}{19n_j}\sum_{a=1}^{19}\sum_{t=1}^{n_j}X_{iajt}(c)\quad\text{for}\quad i=1,2.$$

According to assumption (1),

$$\begin{aligned}\hat{\mu}_{1j}(c) &= \mu_j^F(c)+\frac{1}{19n_j}\sum_{a=1}^{19}\sum_{t=1}^{n_j}\epsilon_{1ajt}(c)\\ \hat{\mu}_{2j}(c) &= \mu_j^F(c)+\mu_j^C(c)+\frac{1}{19n_j}\sum_{a=1}^{19}\sum_{t=1}^{n_j}\epsilon_{2ajt}(c).\end{aligned}$$

A3 Average $PM_{2.5}$ and Its Dependence on Climate Condition

We represent the expectation of $PM_{2.5}$ at a city c as a function of the average meteorological condition μ_X of the city, which is a 9-dimensional vector, via the linear model (8). We will substitute μ_X with either $\mu_{1j}(c)$ and $\mu_{2j}(c)$ to gauge on the effects of the meteorological change on $PM_{2.5}$

Recall that $Y_{aqt}(c,s)$ in model (8) be the log $PM_{2.5}$ level at a monitoring site s at city c in a quarter p that covers or intercept with month j and year a. Then, $Z_{aqt}(c,s)=$

$\exp(Y_{aqt}(c,s))$ be $PM_{2.5}$ in the original scale. Let the average of the meteorological variable $X_{aqt}(c)$ be a generic μ_X, and $\mu_{Y_{aq}}(c,\mu_X)$ be the expectation of $Y_{aqt}(c,s)$.

Then, with $\bar{I} \coloneqq (0.25, 0.25, 0.25)^T$,

$$\begin{aligned}\mu_{Y_{aq}}(c,\mu_X) &= \mathbf{E}[\alpha_{aq}(c) + \beta_{aq}^T(c)X_{aqt}(c) + \eta_{aq}^T(c)I_t + Y_{aq(t-1)}(c,s)\gamma_{aq}(c)] \\ &= \mathbf{E}[\sum_{i=0}^{\infty}\{\alpha_{aq}(c) + \beta_{aq}^T(c)X_{aq(t-i)}(c) + \eta_{aq}^T(c)I_t\}\gamma_{aq}^i(c)] \\ &= \frac{1}{1-\gamma_{aq}(c)}\{\alpha_{aq}(c) + \beta_{aq}(c)^T\mu_X + \eta_{aq}^T(c)\bar{I}\},\end{aligned}$$

which is depends on the average meteorological condition μ_X.

Let $\tilde{\alpha}_{aq}(c) = \alpha_{aq}(c)/(1-\gamma_{aq}(c))$, $\tilde{\beta}_{aq}(c) = \beta_{aq}(c)/(1-\gamma_{aq}(c))$ and $\tilde{\eta}_{aq}(c) = \eta_{aq}(c)/(1-\gamma_{aq}(c))$. Then, an estimator for $\mu_{Y_{aq}}(c,\mu_X)$ is

$$\hat{\mu}_{Y_{aq}}(c,\mu_X) = \hat{\tilde{\alpha}}_{aq}(c) + \hat{\tilde{\beta}}_{aq}^T(c)\mu_X + \hat{\tilde{\eta}}_{aq}^T(c)\bar{I},$$

where $\hat{\tilde{\alpha}}_{aq}(c)$, $\hat{\tilde{\eta}}_{aq}(c)$ and $\hat{\tilde{\beta}}_{aq}(c)$ are estimators by plugging-in the least square regression estimators to $\tilde{\alpha}_{aq}(c)$, $\tilde{\beta}_{aq}(c)$ and $\gamma_{aq}(c)$ in model (8). Since $\hat{\tilde{\eta}}_{aq}^T(c)\bar{I}$ is independent from μ_X as it is for $\tilde{\alpha}_{aq}(c)$. We combine them together by ignoring $\hat{\tilde{\eta}}_{aq}^T(c)\bar{I}$ in the following analysis.

Put $\mu_{Z_{aq}}(c,\mu_X) = E\{Z_{aqt}(c,s)\} = E\{\exp(\hat{\mu}_{Y_{aqt}}(c,s)\}$ be the average $PM_{2.5}$ in the original scale. An initial estimator of $\mu_{Z_{aq}}(c,\mu_X)$ is $\hat{\mu}_{Z_{aq}}(c,\mu_X) = \exp(\hat{\mu}_{Y_{aq}}(c,\mu_X))$.

A4 Meteorological Change Effects Estimation

We define meteorological change effect in month j and year a at city c as

$$\widehat{\Delta Z_{aj}}(c) = \hat{\mu}_{Z_{aq}}(c,\hat{\mu}_{2j}(c)) - \hat{\mu}_{Z_{aq}}(c,\hat{\mu}_{1j}(c)), \tag{A2}$$

which is the difference in the expectations of raw $PM_{2.5}$ under the average meteorological condition between the two time periods. Here, p is the time segment that month j falls into or intercept with. The latter case includes March and November, which we will use the average of the two adjacent time segments to measure the meteorological change effect.

We carry a bias correction to the estimator in (A2) to offset the non-linearity in the exponential transformation. Let $\hat{\xi}_{aj}(c) = (\hat{\mu}_{1j}^T(c), \hat{\mu}_{2j}^T(c), \hat{\tilde{\alpha}}_{aq}(c), \hat{\tilde{\beta}}_{aq}^T(c))^T$, $\xi_{aj}(c) = E(\hat{\xi}(c)) = (\mu_j^{FT}(c), \mu_j^{FT}(c) + \mu_j^{CT}(c), \tilde{\alpha}_{aq}(c), \tilde{\beta}_{aq}^T(c))^T$. Let $h_1(x) = e^{x_3 + x_4^T x_1}$, $h_2(x) = e^{x_3 + x_4^T x_2}$ and $h(x) = h_2(x) - h_1(x)$. Then, $h(\hat{\xi}_{aj}(c)) = \widehat{\Delta Z_{aj}}(c)$.

For $\widehat{\Delta Z_{aj}}(c)$, a Taylor expansion near $\xi_{aj}(c)$ gives

$$\widehat{\Delta Z_{aj}}(c) \approx h(\xi_{aj}(c)) + \nabla h(\xi_{aj}(c))^T(\hat{\xi}_{aj}(c) - \xi_{aj}(c)) + \frac{1}{2}(\hat{\xi}_{aj}(c) - \xi_{aj}(c))^T\nabla^2 h(\xi_{aj}(c))(\hat{\xi}_{aj}(c) - \xi_{aj}(c)).$$

The expectation of $\widehat{\Delta Z_{aj}}(c)$ is approximately

$$E(\widehat{\Delta Z_{aj}}(c)) \approx h(\xi_{aj}(c)) - \frac{1}{2}\mathrm{tr}(\nabla^2 h(\xi_{aj}(c))E((\hat{\xi}_{aj}(c) - \xi_{aj}(c))(\hat{\xi}_{aj}(c) - \xi_{aj}(c))^T)).$$

The bias corrected estimation of $\widehat{\Delta Z_{aj}}(c)$ is

$$\widehat{\Delta \tilde{Z}_{aj}}(c) = \hat{\mu}_{Z_{aq}}(c,\hat{\mu}_{2j}(c)) - \hat{\mu}_{Z_{aq}}(c,\hat{\mu}_{1j}(c)) + \frac{1}{2}\mathrm{tr}[\nabla^2 h(\hat{\xi}_{aj}(c))\widehat{\mathrm{Var}}(\hat{\xi}_{aj}(c))]. \tag{A3}$$

The first and second order gradient of $h(x)$ are

$$\nabla h(x) = \begin{pmatrix} -x_3 h_1(x) \\ x_4 h_2(x) \\ h(x) \\ x_2 h_2(x) - x_2 h_1(x) \end{pmatrix} \quad \text{and}$$

$$\nabla^2 h(x) = \begin{pmatrix} -x_4 x_4^T h_1(x) & 0 & -x_4 h_1(x) & -(I + x_4 x_4^T) h_1(x) \\ 0 & x_4 x_4^T h_2(x) & x_4 h_2(x) & (I + x_4 x_4^T) h_2(x) \\ -x_4^T h_1(x) & x_4^T h_2(x) & h(x) & x_2^T h_2(x) - x_1^T h_1(x) \\ -x_1 x_4^T h_1(x) & x_2 x_4^T h_2(x) & x_2 h_2(x) - x_1 h_1(x) & x_2 x_2^T h_2(x) - x_1 x_1^T h_1(x) \end{pmatrix}.$$

For the variance of $\hat{\xi}_{aj}(c)$, it can be shown that

$$\mathrm{Var}(\hat{\xi}_{aj}(c)) = \begin{pmatrix} \mathrm{Var}(\hat{\mu}_{1j}(c)) & 0 & 0 \\ 0 & \mathrm{Var}(\hat{\mu}_{2j}(c)) & 0 \\ 0 & 0 & \mathrm{Var}((\hat{\tilde{\alpha}}_{aq}(c), \hat{\tilde{\beta}}_{aq}^T(c))) \end{pmatrix}.$$

Thus, its estimation can be attained by separately estimating the three diagonal covariances, say $\widehat{\mathrm{Var}}(\hat{\mu}_{1j}(c))$, $\widehat{\mathrm{Var}}(\hat{\mu}_{2j}(c))$ and $\widehat{\mathrm{Var}}((\hat{\tilde{\alpha}}_{aq}(c), \hat{\tilde{\beta}}_{aq}^T(c)))$.

Note that $\mathrm{Var}(\hat{\mu}_{ij}(c)) = \frac{1}{19}\mathrm{Var}(\frac{1}{n_j}\sum_{t=1}^{n_j} \epsilon_{iajt}(c))$, where n_j is the number of observations in month j of a year. Let $\tilde{\epsilon}_{iajt}(c) = X_{iajt}(c) - 18^{-1}\sum_{a' \neq a} X_{ia'jt}(c) = \epsilon_{iajt}(c) - 18^{-1}\sum_{a' \neq a} \epsilon_{ia'jt}(c)$ and $\tilde{\Sigma}_{ij}(c) = \mathrm{Var}(\frac{1}{n_j}\sum_{t=1}^{n_j} \tilde{\epsilon}_{iajt}(c))$. Then $\tilde{\Sigma}_{ij}(c) = 19\Sigma_{ij}(c)/18$, where $\Sigma_{ij}(c) = \mathrm{Var}(\frac{1}{n_j}\sum_{t=1}^{n_j} \epsilon_{iajt}(c))$. Let $\widehat{\tilde{\Sigma}_{ij}(c)}$ be the block bootstrap estimator of $\tilde{\Sigma}_{ij}(c)$ (Küunsch, 1989). Then, $\widehat{\mathrm{Var}}(\hat{\mu}_{ij}(c)) = 18\widehat{\tilde{\Sigma}_{ij}}(c)/19^2$. The variance of $(\hat{\tilde{\alpha}}_{aq}(c), \hat{\tilde{\beta}}_{aq}(c))$ can be obtained via the sieve bootstrap (Bühlmann, 2002) for time series regression models.

A5 Estimating the Variance of Meteorological Change Effects

By ignoring the second order term in (A3), the variance of $\widehat{\Delta\tilde{Z}_{aj}}(c)$ is approximated by applying the delta method

$$\mathrm{Var}(\widehat{\Delta\tilde{Z}_{aj}}(c)) \approx \nabla h(\hat{\xi}_{aj}(c))^T \mathrm{Var}(\hat{\xi}_{aj}(c)) \nabla h(\hat{\xi}_{aj}(c)),$$

which can be estimated by plugging in $\nabla h(\hat{\xi}_{aj}(c))$ and $\widehat{\mathrm{Var}}(\hat{\xi}_{aj}(c))$.

A6 Estimating Regional Average Meteorological Change Effect and its Variance

The regional average meteorological change effect is given by

$$\hat{\eta}_{aj} = \frac{1}{32}\sum_{c=1}^{32} \widehat{\Delta\tilde{Z}_{aj}}(c).$$

Let $\hat{\xi}_{aj} = (\hat{\xi}_{aj}(1), \cdots, \hat{\xi}_{aj}(32))^T$ and $g(x) = \frac{1}{32}\sum_{c=1}^{32} h(x_c)$. Then, $\hat{\eta}_{aj} = g(\hat{\xi}_{aj})$. Its variance can be approximated by the delta method

$$\begin{aligned} \mathrm{Var}(\hat{\eta}_{aj}) &= \mathrm{Var}(g(\hat{\xi}_{aj})) \\ &\approx \nabla g^T(\hat{\xi}_{aj}) \mathrm{Var}(\hat{\xi}_{aj}) \nabla g(\hat{\xi}_{aj}), \end{aligned}$$

where $\nabla g^T(x) = (\nabla h^T(x_1), \cdots, \nabla h^T(x_{32}))/32$.

We partition $\mathrm{Var}(\hat{\xi}_{aj})$ into 32×32 block matrices with (p, q)-th block matrix being

$$\mathrm{Var}(\hat{\xi}_{aj})_{pq} = \mathrm{Cov}(\hat{\xi}_{aj}(p), \hat{\xi}_{aj}(q)).$$

The cases for $p = q$ have been discussed in the previous subsection. When $p \neq q$, it can be shown that

$$\mathrm{Cov}(\hat{\xi}_{aj}(p), \hat{\xi}_{aj}(q)) = \begin{pmatrix} \mathrm{Cov}(\hat{\mu}_{1j}(p), \hat{\mu}_{1j}(q)) & 0 & 0 \\ 0 & \mathrm{Cov}(\hat{\mu}_{2j}(p), \hat{\mu}_{2j}(q)) & 0 \\ 0 & 0 & 0 \end{pmatrix}.$$

Its estimation can be attained by estimating $\widehat{Cov}(\hat{\mu}_{1j}(p), \hat{\mu}_{1j}(q))$ and $\widehat{Cov}(\hat{\mu}_{2j}(p), \hat{\mu}_{2j}(q))$, with the block bootstrap method, the method we have used earlier.

It can be shown that $\hat{\eta}_{aj}$ is asymptotically distributed, which leads to the confidence interval in Figure 5 (b).

Figure1.

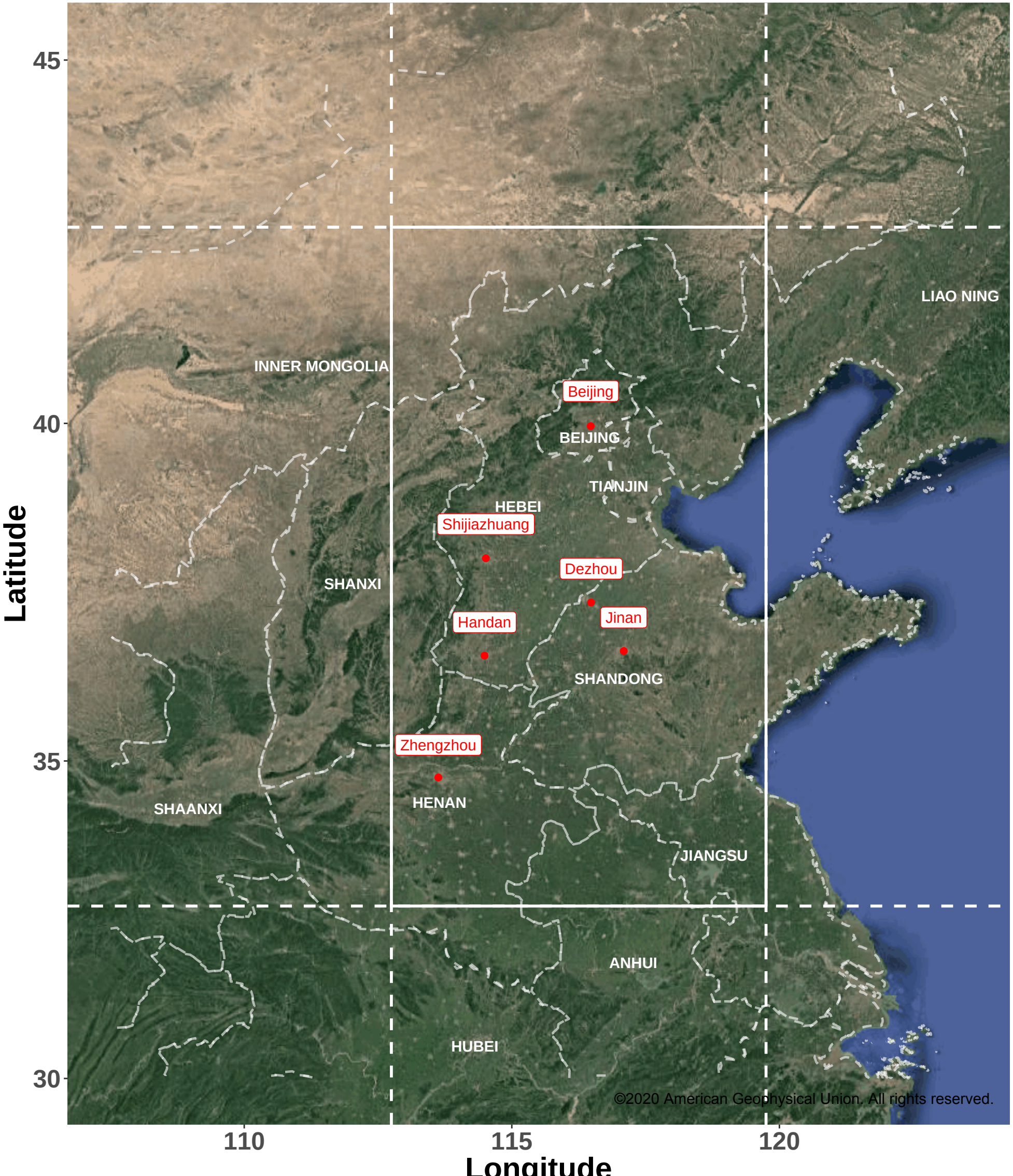
45
40
35
30
Latitude
110
115
120
Longitude
INNER MONGOLIA
LIAO NING
Beijing
BEIJING
TIANJIN
HEBEI
Shijiazhuang
Dezhou
Jinan
Handan
SHANDONG
Zhengzhou
HENAN
SHAANXI
JIANGSU
ANHUI
HUBEI
SHANXI
©2020 American Geophysical Union. All rights reserved.

Figure2.

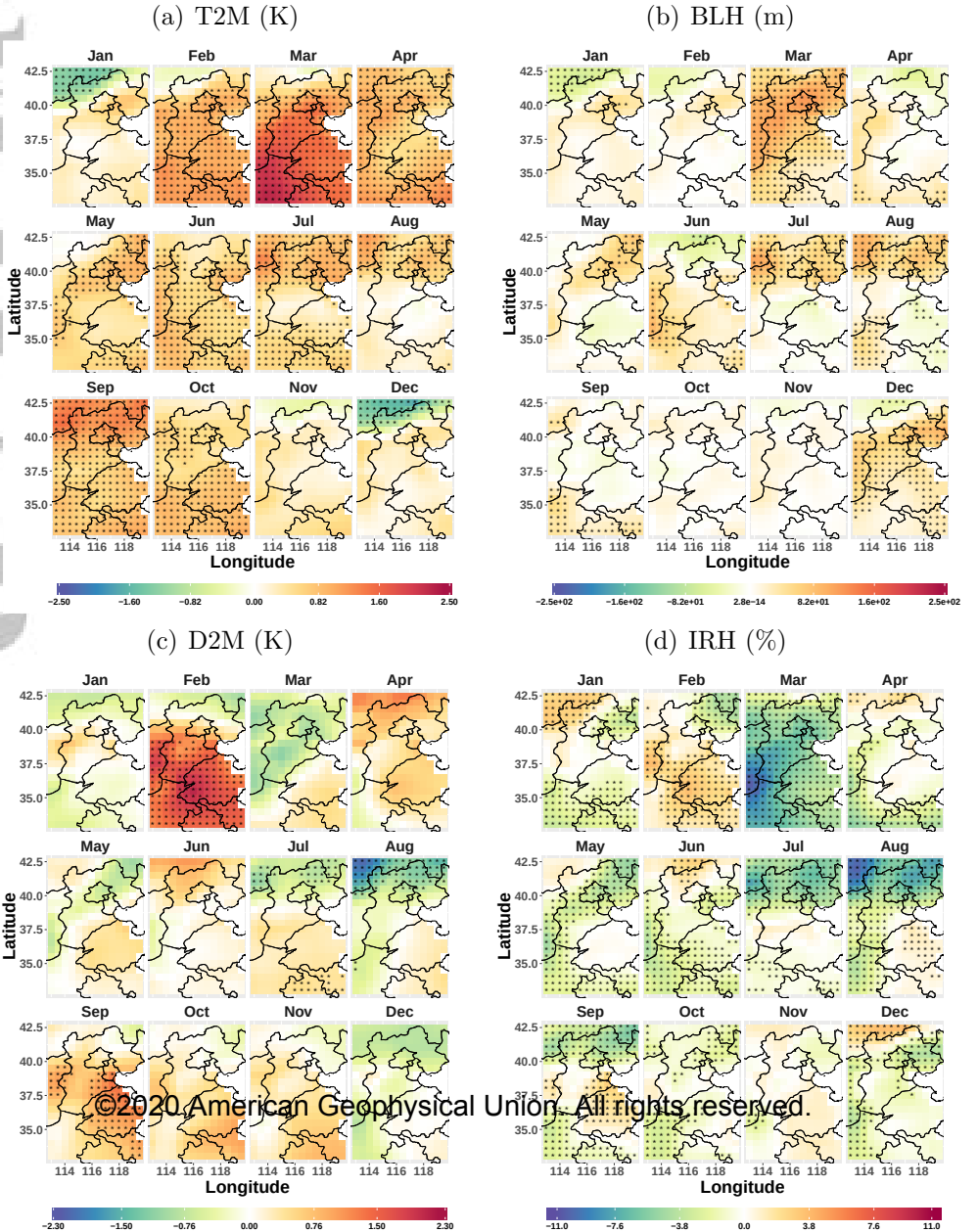

Figure3.

(a) Integrated NW (m/s)

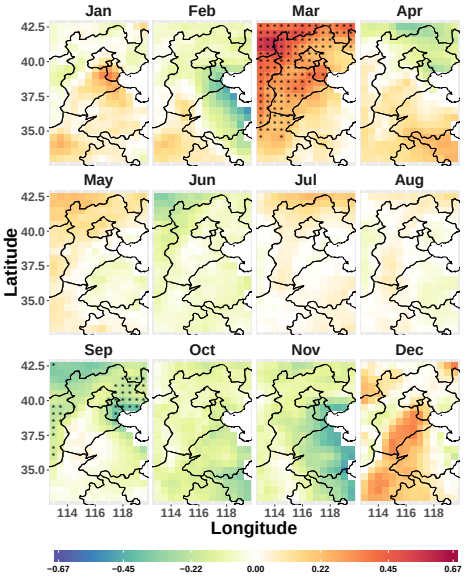

(b) Integrated NE (m/s)

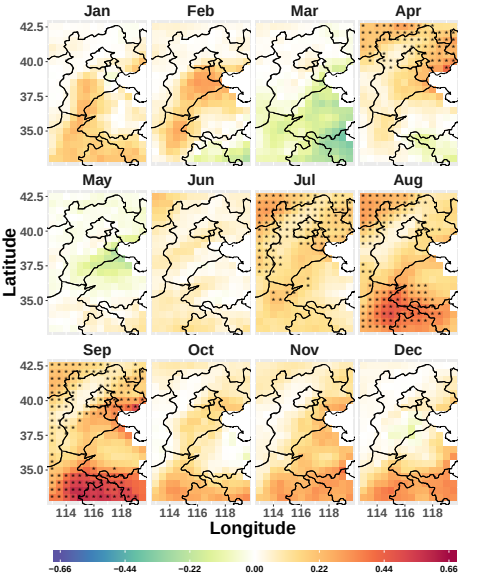

(c) Integrated SW (m/s)

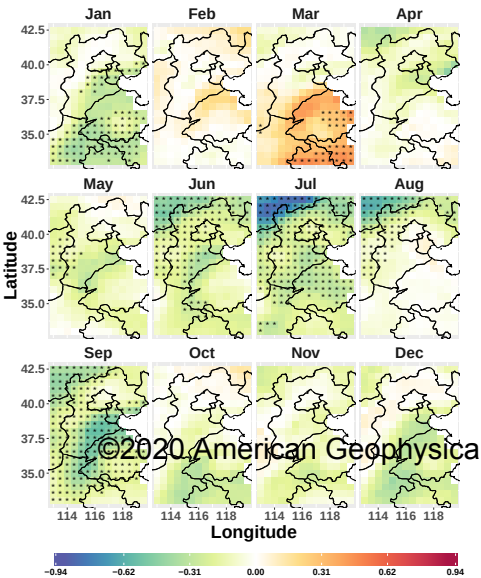

(d) Integrated SE (m/s)

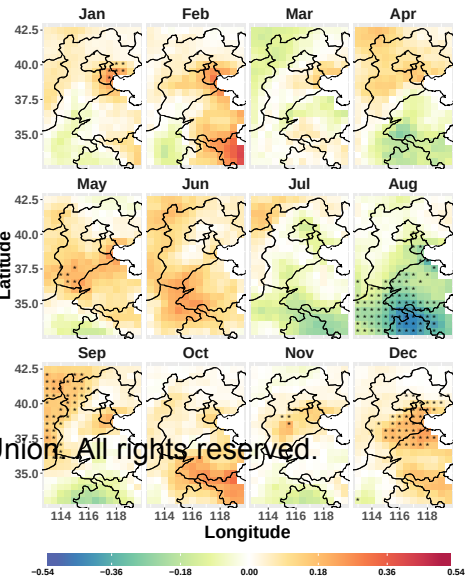

Figure4.

(a) 2014

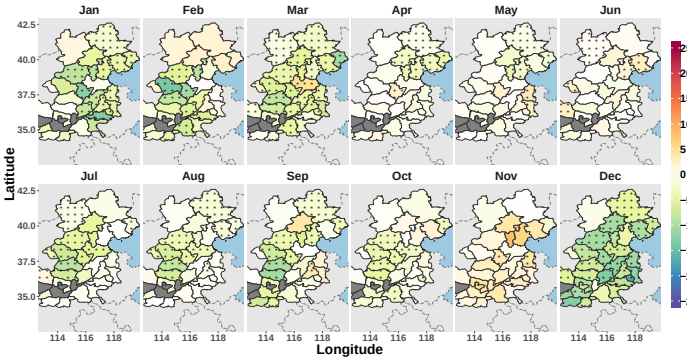

(b) 2015

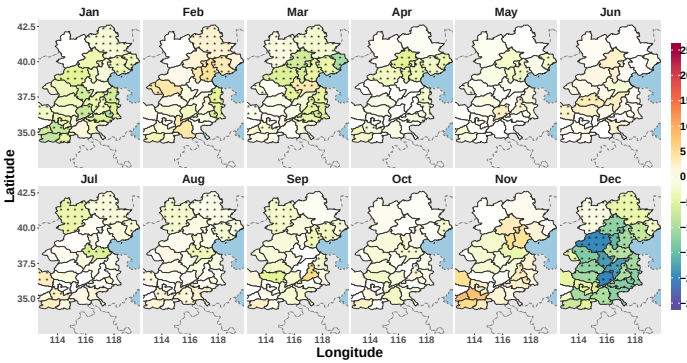

(c) 2016

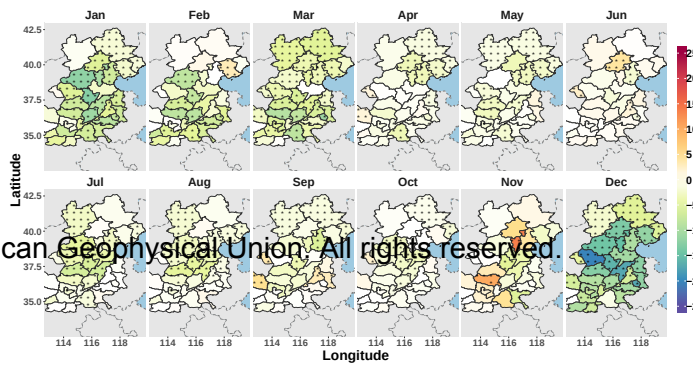

Figure5.

(a)

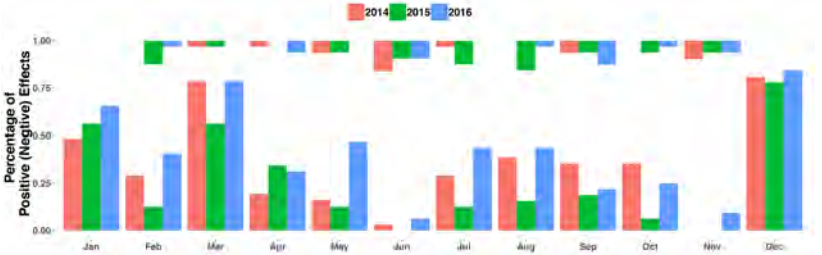

(b)

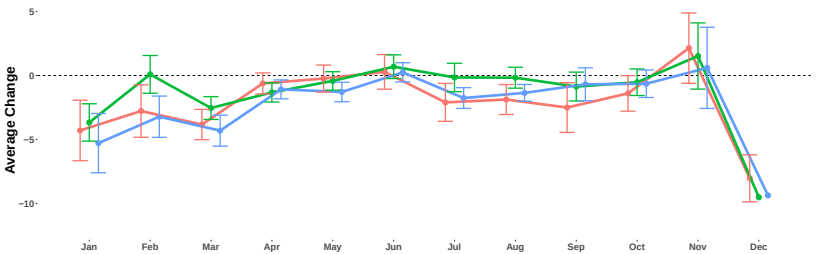

(c)